Different Approaches to the Analysis of Complex Molecular Dynamics

Arnulf Materny

Jacobs University Bremen
Campus Ring 1, 28759 Bremen, Germany
a.materny@jacobs-university.de

January 23, 2009

Contents

1 Summary

In this lecture some basics of spectroscopy in "femtochemistry" are discussed. Femtochemistry is about the investigation and control of ultrafast elementary molecular dynamics, which are the basis of every chemical reaction. The processes finally resulting in breaking and forming of chemical bonds or in molecular structure changes take place within only femtoseconds to picoseconds. Therefore, only femtosecond laser pulses are fast enough to resolve these fast dynamics. Different techniques were developed, which make use of the combination of femtosecond pulses having variable relative time delays, in order to gain access to the dynamics even in complex molecules. The knowledge of the elementary processes allows for a better understanding of the reaction mechanisms and their dependence on environmental conditions. In this lecture an overview is given of techniques, which can be applied for the investigation of ultrafast molecular dynamics. Since during the last three decades a considerable number of different approaches has been developed, only a selection will be introduced here. Nevertheless, the lecture should give enough insight into the principle ideas behind the analysis of processes on an elementary time scale. Special emphasis is put on concrete examples, which are supposed to demonstrate how certain spectroscopic methods can be applied to real molecular systems.

The lecture should be considered to be an introduction into femtosecond time-resolved spectroscopy also for readers not so familiar with the basic concepts (*e.g.* undergraduate students). Therefore, more advanced theoretical interpretations will be avoided (for more theoretical background information, *e.g.* see the very nice contribution by Prof. Hamm, "... Mukamel for Dummies"). However, also more advanced students should find new information in the text.

2 Introduction

For the characterization of chemical reactions, reaction equations are used.

$$A + BC \longrightarrow AB + C \tag{1}$$

These reaction equations characterize the chemical process by giving the reactants and the products for the single reaction steps. The arrow seems to only define the direction of the reaction path. However, besides the macroscopic world of reactants and products there also exists a variety of microscopic aspects, which are hidden behind the reaction arrow, finally determining what product will result from the reaction. Chemical bonds break and form, or they change their geometry with huge velocity. Typically, the atomic building blocks of molecules within a millionth of a second cover a distance of approximately 1 mm. Therefore, the dynamics on an atomic length scale of few angstroms take place on a femtosecond time scale. One femtosecond is the billionth of a millionth of a second (1 fs = 10^{-15} s), an incredibly short time, during which light only travels 0.3 μm. Only "femtochemistry" yielded the observation of these fundamental processes in real time. This research field, which is found between Chemistry and Physics, deals with both the observation and the control of elementary motion of atoms within the molecules (reactants) while they are rearranging to form new molecules (products).

Here, we mainly will concentrate on the observation of ultrafast intra and intermolecular dynamics. Before we discuss some examples of experimental techniques, we first should consider some fundamentals.

2.1 The Transition State

Before "femtochemistry" was established, more than a century of intense research work anteceded, in which scientists tried to gain deeper going understanding of the elementary processes during chemical reactions. The first quantitative measurement of reaction kinetics was reported in 1850 by Ludwig Wilhelmy. He investigated the inversion of sugar where a solution of sucrose is hydrolyzed into glucose and fructose. Svante Arrhenius (1859–1927, Nobel Prize in Chemistry 1903) found that many chemical reactions have to be activated, even when they proceed exothermically *i.e.* releasing energy. Here, the reaction path has to overcome a potential energy maximum, the hight of which is given by the "activation energy". This molecular transition state was called by Arrhenius "activated complex" (see Fig. 1). The famous equation given by Arrhenius, which partially was based on earlier work by Jacobus H. van't Hoff (1852–1911, Nobel Prize in Chemistry 1901), describes the rate constant of the reaction, k as a function of temperature:

$$k = A\, e^{-E_a/RT}\,. \tag{2}$$

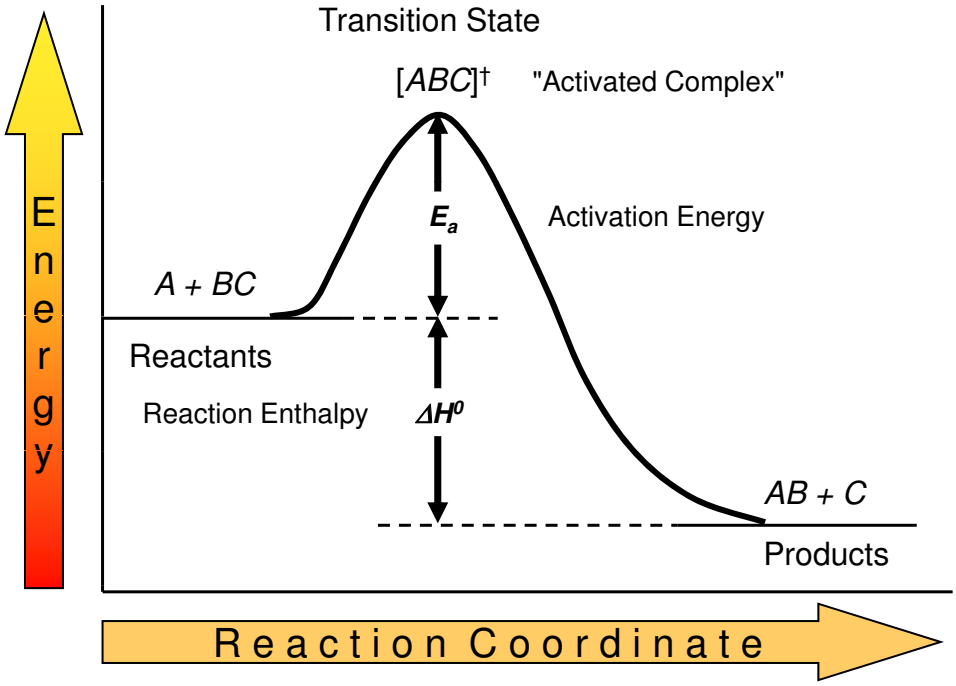

Figure 1: *In this example, the energies of the products are less compared to those of the reactants. This means that during the reaction energy (reaction enthalpy ΔH^0) is released (exothermic reaction). Nevertheless, the chemical process does not start before an activation energy E_a is supplied. This energy is needed for the system to overcome the energy barrier. Along this reaction path the transition state is formed, the "activated complex". The goal of femtochemistry is the observation and/or the control of this chemically important intermediate step.*

In this equation R is the universal gas constant, T is the absolute temperature in Kelvin, and E_a the above mentioned activation energy. While the Arrhenius equation described macroscopic kinetics of molecule ensembles, in 1931 Henry Eyring (1901–1981) and Michael Polanyi (1891-1976) [1] succeeded in developing a microscopic model for the dynamics of single molecules. In their work they calculated the potential energy surface of the reaction H + H_2 and described the path of the educt's nucleus across the decisive transition state of the activated complex towards the product. In 1935 Eyring [2] as well as Evans and Polanyi [3] independent of each other formulated the theory of the transition state. This theory allowed for the estimation of the reaction rate. According to this, the transition state between educt and product will be passed on the time scale of a molecular vibration, *i.e.* within several femtoseconds. Now, also the pre-exponential factor A of the Arrhenius equation could be explained; it especially depends on the geometric arrangement of the reacting molecules.

The transition state, which only exists for such a short time, nevertheless constitutes the

decisive moment for the reaction dynamics. If one reconsiders the simple reaction given in Equ. 1,

$$A + BC \longrightarrow [ABC]^{\ddagger} \longrightarrow AB + C\,, \tag{3}$$

the nuclear distances change typically by something on the order of 10 Å. This means, the reaction time will be on the order of 1–10 picoseconds (1 ps = 1000 fs). If one is interested in the observation of the activated complex $[ABC]^{\ddagger}$, then a spatial resolution of 0.1 Å appears to be sensible, which is equivalent to a temporal resolution of 10–100 fs.

Now, different questions arise. How can experimental observations on such short time scales be realized? What do we have to take into consideration when doing such experiments? Which processes can be observed? Can we take influence on the elementary molecular dynamics? In short, what is Femtochemistry and what can it do?

2.2 Some History ...

The idea to take snapshots of molecules while they are reacting is attractive. In the second half of the 19^{th} century the photographer Eadweard Muybridge succeeded in taking a fast series of photographs, demonstrating that a galloping horse temporarily looses contact with the ground with all for hooves (see Fig. 2). The actual temporal resolution was approximately 10^{-3} s. Of course, the shutter speeds of cameras are far from the desired femtosecond time window and imaging techniques in terms of photography also fail for the extremely small actors. Therefore, alternative techniques have to be found.

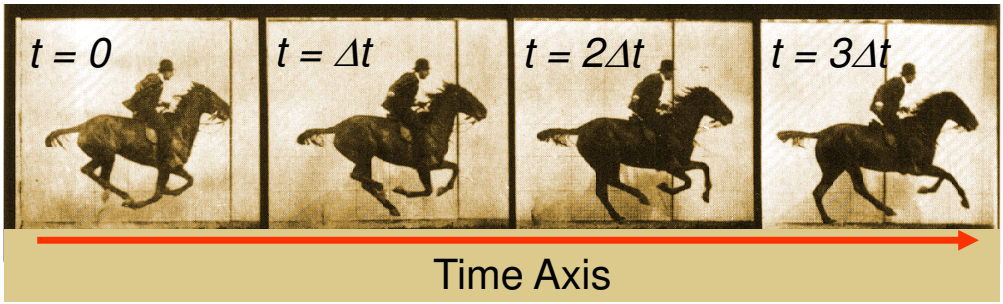

Figure 2: *The photos were taken by the English photographer, Eadweard Muybridge, to settle a bar bet between California's Governor Leland Stanford and some of his friends. Stanford claimed that at some point in a horse's stride, all four hooves were off the ground. Muybridge's pictures showed that Stanford had won the bet. The temporal resolution achieved was approximately 10^{-3} s.*

In 1967 Manfred Eigen, Ronald Norrish, and George Porter received the Nobel Prize in Chemistry "for their studies of extremely fast chemical reactions, effected by disturbing the

equilibrium by means of very short pulses of energy". The shortly after World War II developed flash photolysis opened the door to the investigation of dynamics in the microsecond range [4]. Finally, the realization of the laser by Theodore Maiman in 1960 resulted in the development of a "mode coupled" laser in 1974 by Charles Shank and Erich P. Ippen [5] capable of emitting light pulses with lengths in the femtosecond regime. Nowadays, lasers with pulse durations of few femtoseconds are commercially available.

The first to utilize the ultrashort laser pulses to gain access to the transition state of chemical reactions was the US scientist Ahmed H. Zewail. In 1987, the native-born Egyptian investigated the light-induced dissociation of iodocyanide (ICN) into iodine (I) and cyanide (CN) [6]. The observed reaction time was only 200 fs. Zewail established femtochemistry and finally, in 1999 received the Nobel Prize in Chemistry "for his studies of the transition states of chemical reactions using femtosecond spectroscopy".

2.3 Some Fundamentals ...

An important issue for the measurement of dynamics is the determination of a starting point in time. This means that in order to follow the course of *e.g.* a chemical reaction, the time of inducing the reaction has to be as precisely known as the time of probing the following dynamics. For this a "pump-probe" technique has to be used. With the pump step, a laser pulse (or a combination of several laser pulses) excites the molecule into a higher lying energy state, which is the starting point of the chemical reaction or also non-reactive molecular dynamics. After a variable time delay, a further laser pulse (or a combination of several laser pulses) interrogates the active state of the system. This probe step has to result in a probe and system specific signal, which then gives information about the transient molecular state.

It is important to point out two important facts, which considerably restrict femtochemistry. Firstly, the necessity of having to start the dynamics by using the interaction between an ultrafast laser pulse and the molecules limits the investigations to photochemically active systems. Processes, which start without the initiation by photons like collision-induced reactions at most can be measured in an indirect way. Secondly, one finds that the selective probing of reaction dynamics in many cases is an extremely challenging and in too many cases up to now unsolved task. Usually, the interaction of the probe laser with the molecule induces processes, which reflects the present state of the system under investigation. A typical example is the light-induced fluorescence. Here, selectivity regarding the transient structure of the molecules or the activated complex can be achieved by making use of resonant transitions into a higher energy state of the molecule, which finally emits fluorescence. Of course the existence of such states can not be guaranteed for all molecules. Using a variety of different probe (and pump) techniques (mass spectrometry after laser-induced ionization, transient absorption, etc.) researchers try to overcome this limitation. Some of these techniques will be discussed below. Others, like the use of X-ray [7] and electron scattering [8]

used for a more direct access to the dynamics of structural changes are highly specialized and would be part of a separate lecture.

Before we learn about examples of time-resolved investigations of reaction and molecular dynamics, some further fundamental properties of femtosecond spectroscopy have to be discussed.

Femtosecond laser pulses are extremely short and such well-defined on the time scale. However, laser light is also characterized by its spectral position and width. The relation between time and energy domain is given by the Fourier transform theory. The Fourier formula assigns to the temporal profile $A(t)$ of the shortest possible pulse a corresponding spectral profile $\tilde{A}(\nu)$ as function of the light frequency ν. The Fourier transform gives the relation between these two functions in both directions (forward and inverse transform):

$$\tilde{A}(\nu) = \frac{1}{\sqrt{2\pi}} \int_{-\infty}^{\infty} A(t) e^{-i\nu t} dt \quad \longleftrightarrow \quad A(t) = \frac{1}{\sqrt{2\pi}} \int_{-\infty}^{\infty} \tilde{A}(\nu) e^{i\nu t} d\nu \,. \tag{4}$$

As a consequence of this relation, also a limiting rule can be derived for the femtosecond pulses. This means that between the temporal width Δt of the pulse and its spectral width $\Delta\nu$ a relation exists, which is similar to the Heisenberg uncertainty relation known for space and momentum:

$$\Delta t \cdot \Delta\nu \geq K \,. \tag{5}$$

The constant K depends on the pulse shape. For Gaussian pulses the value of K is approximately 0.441. Therefore, ultrashort femtosecond laser pulses are spectrally broad. A 100-fs laser pulse centered around a wavelength of 500 nm according to this would at least have a spectral full width at half maximum of approximately 8 nm. The continuous wave (cw) argon-ion lasers typically used for frequency resolved laser spectroscopy feature about three orders of magnitude narrower emission line widths.

The considerable spectral width of the femtosecond laser pulses entails important consequences for time domain spectroscopy. Without going into too much detail, nevertheless, the principle of "coherence" shall be shortly discussed. Molecular states are characterized by their wave functions, *i.e.* the solutions of the Schrödinger equation. Quantum mechanics states that only the absolute squares of these functions can be observed in experiments. It can be easily shown that for a single eigen function $\Psi(r,t)$ the temporal component is lost.

$$\Psi(r,t) = \Psi(r) e^{-i\omega t} \quad \longrightarrow \quad |\Psi(r,t)|^2 = \Psi(r,t)\Psi^*(r,t) = |\Psi(r)|^2 \neq f(t) \,. \tag{6}$$

Therefore, it is impossible to observe the temporal behavior of a single molecular state. Nevertheless, the motion of molecules can be accessed in real-time. This is directly related to the spectral width of the laser pulses. The interaction of the femtosecond laser pulse with

the molecule will not only interact with a single state, but several *e.g.* vibrational states will be excited coherently, *i.e.* in phase. The superposition of the corresponding wave functions results in beating phenomena or "wave packets" (in our example a vibrational or nuclear wave packet), which performs a classical motion along the nuclear coordinate (see Fig. 3). This wave packet (or beating) can be followed in time and thus gives information about the molecular or reaction dynamics.

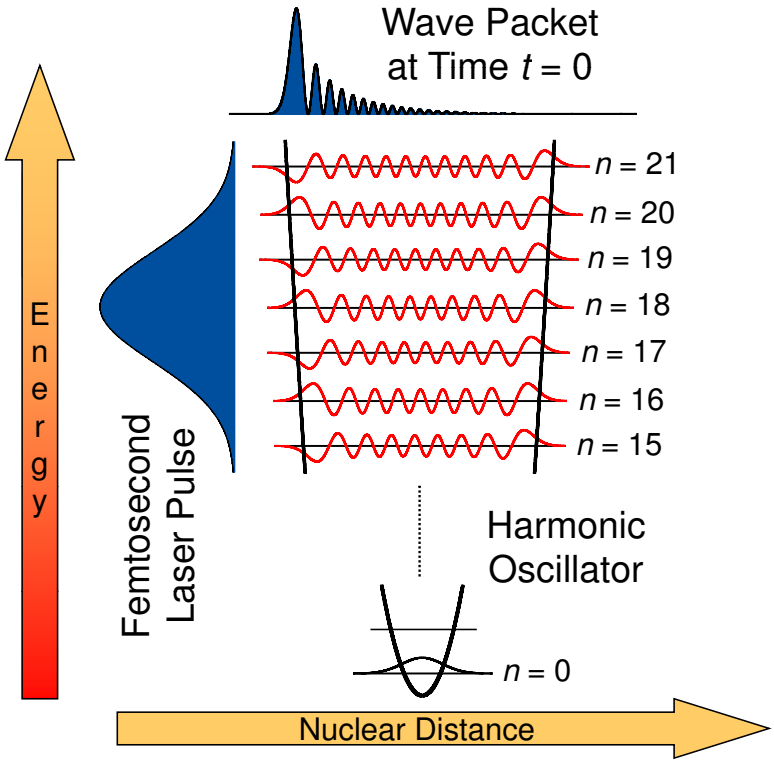

Figure 3: *Femtosecond laser pulses are very short but spectrally rather broad as follows from the Fourier transform relation. As consequence, the interaction with molecules not only results in the excitation of single eigen states but rather in the transition into several molecular states. In the scheme this is shown for a harmonic oscillation. The pump laser coherently superimposes a number of vibrational overtone states. This excitation of eigen functions with well-defined phases results in a wave packet, which moves like a classical particle with the frequency of the molecular vibration. With the help of femtosecond time-resolved laser spectroscopy this motion can be observed and also influenced.*

Let us shortly go into a mathematical description of this coherence phenomena. The coherent broadband excitation makes the state function a sum of stationary wave functions for different energies E_i but with well-defined phase relations. A general superposition of wave functions would be described by

$$\Psi(r,t) = \sum_i c_i \Psi_i(r) \exp(-iE_i t/\hbar + \varphi_i) \quad \text{where} \quad E_i/\hbar = \omega_i \,. \tag{7}$$

The coefficients c_i determine the relative amplitudes of the contributing wave functions and φ_i is a constant describing the relative phase shift. If the excitation is coherent, the phase shift constants φ_i can all be set to zero and such in the experiment the observed absolute square is a wave packet, which oscillates with frequencies determined by the energy differences $E_i - E_j$:

$$|\Psi(r,t)| = \Psi(r,t)\Psi^*(r,t) = \left[\sum_i c_i \Psi_i(r) \exp(-iE_i t/\hbar)\right]\left[\sum_j c_j \Psi_j(r) \exp(-iE_j t/\hbar)\right] \tag{8}$$

Here, only the cross-terms ($i \neq j$) have a temporal dependence, while for the diagonal elements the phase factors cancel.

3 Linear and Nonlinear Femtosecond Time-Resolved Spectroscopy

In literature more and more new techniques are introduced, which are used to most efficiently excite molecular or reaction dynamics and – even more – to probe the partly complex processes. Especially for big molecular systems like biomolecules selective probing of dynamics is extremely demanding due to the many pathways opening after a molecular excitation. Only some will be discussed in the following. The simplest way to approach time domain problems is the use of a two-laser pulse pump-probe method. For many systems a wealth of information can be gained from this.

3.1 Two-Pulse Pump-Probe Spectroscopy — The NaI Experiment

Meanwhile, a huge number of articles has been published, reporting about femtosecond time-resolved spectroscopy on many different systems, beginning with simple diatomic molecules to complex biological systems. Some of the most beautiful examples originate from the work group of the inventor of femtochemistry, Ahmed Zewail, himself. In one of his first experiments, the nuclear motion of gaseous sodium iodide (NaI) during the photo-induced dissociation could be successfully observed via the wave packet dynamics [9, 10]. During the experiment, the NaI is characterized by an ionic (electronic ground state) or covalent bonding (electronic excited state). The ionic bond is caused by the electrostatic attraction between the Na^+ and I^- ions, while for the covalent linkage (also atomic or electron-pair bond) the interaction between the Na and I atoms is responsible. In Fig. 4 on the left

side a simplified potential energy scheme of NaI is displayed. The shown potential curves represent the potential energies of the molecule as functions of the nuclear distance for different electronic configurations. The molecule is bound for closed potential wells. Here, an oscillatory behavior between to turning points (maximum potential energy, minimum kinetic energy) can be found, reflecting the molecular vibration. If the potential energy curve is open on the right side, the nuclear motion finally leads to a breaking of the molecular bond (dissociation). In the experiment the pump laser pulse with photon energy $h\nu_{pu}$ excites the molecule from its electronic ground to the first excited state preparing a coherent wave packet there. Contrary to the purely dissociative reaction expected due to the repulsive excited state, the reaction of NaI

$$\mathrm{Na^+I^-} \xrightarrow{h\nu_{pu}} \mathrm{NaI^*} \longrightarrow [\mathrm{Na} \cdots \mathrm{I}]^{\ddagger *} \longrightarrow \mathrm{Na} + \mathrm{I}$$

is characterized by the "avoided crossing" between the ionic ground state ($\mathrm{Na^+I^-}$) and the covalent excited state ($\mathrm{NaI^*}$, the asterisk marking an electronic excitation). This property of all alkali halides results in an interesting behavior of the wave packet.

Since there is a strong interaction between the crossing potential curves an energy barrier exists. This results in the formation of a quasi-bound potential energy curve ("adiabatic potential") from parts of ground and excited state potentials. Within this adiabatic potential the wave packet oscillates hence and forth. The barrier has limited energy and therefore only delays the dissociation to sodium and iodine atoms in their electronic ground states. Every time, the wave packet passes the avoided crossing, part of it is tunneling through the barrier and follows the path of the undisturbed potential ("diabatic potential") resulting in the breaking of the NaI bond. Interestingly, both oscillation and dissociation are accompanied by electron transfer between the bonding partners (covalent and ionic bond).

How can we now follow this dynamics in an experiment with temporal and spatial resolution? This is the task of the selective probe process. Here, a time-delayed femtosecond laser pulse probing the system allows for the time resolution. The probing of the wave packet at well-defined inter-nuclear distances (nuclear coordinate, reaction coordinate) is achieved by making use of resonance conditions. For the NaI molecule a transition to an even higher lying electronic state is utilized. This state is repulsive and results in the decay of the molecule into iodine atoms in their ground state and electronically excited sodium atoms ($\mathrm{Na^*}$). The latter finally emit the Na-D fluorescence at approximately 589 nm when $\mathrm{Na^*}$ relaxes back into its ground state. The fluorescence of course only will be observed, when the probe interaction with the wave packet takes place at the right time (delay time between pump and probe pulses) and at the right nuclear coordinate (resonance condition). Therefore, the intensity of the fluorescence signal measured as a function of the delay time between the laser pulses as well as of the wavelength of the probe laser reflects the dynamics of the excited sodium iodide ($\mathrm{NaI^*}$) via the transition state $[\mathrm{Na} \cdots \mathrm{I}]^{\ddagger *}$ towards the products Na + I.

The right panels of Fig. 4 show transients for two different probe wavelengths. For 620 nm (λ^*_{pr}) (top right panel) the resonant transition lies in the range of the adiabatic potential.

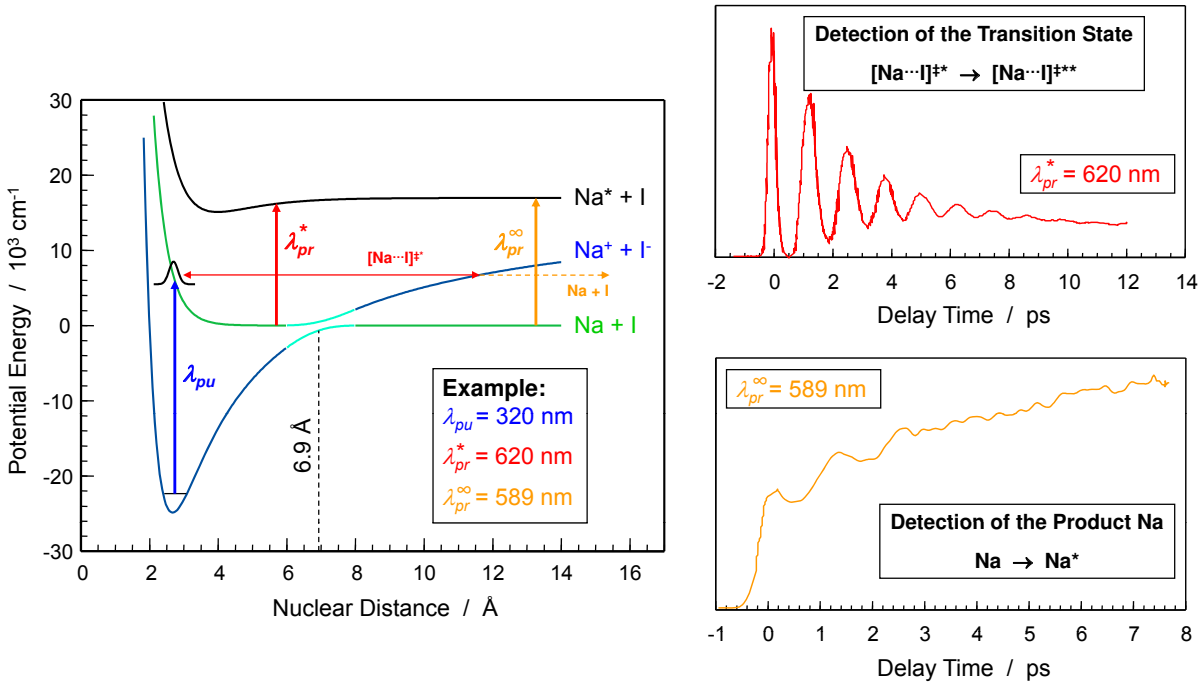

Figure 4: *Sodium iodide (NaI) is an interesting molecule. While the molecule in its electronic ground state (blue curve) has an ionic bond, the first excited electronic state (green curve) is characterized by a covalent bond. The latter state is repulsive, i.e. the molecule decays into its atomic components sodium and iodine. However, due to the symmetry of the molecular states, the two potentials undergo an "avoided crossing". Parts of the ground and excited states form new (adiabatic) potentials (shown as turquoise intermediate pieces). Now, the excited state is a bounding state, where the molecule oscillates between covalent and ionic bonding conditions. However, with a certain probability, the wave packet tunnels to the repulsive (diabatic) potential branch at the potential crossing, resulting in a dissociation reaction. In the femtosecond experiment depending on the probe wavelength the wave packet can be observed either on the adiabatic potential energy surface (λ^*_{pr}) or while moving along the diabatic potential branch (λ^∞_{pr}). Thus, the transition state and the production of sodium and iodine atoms can be observed, respectively. The detection is via the fluorescence (Na-D line) emitted after the probe laser has excited the NaI molecule in a higher lying repulsive state resulting in excited sodium atoms. The left panel shows the different potential curves with their respective dissociation products. Here, Na* labels the excited state of the sodium atom, which emits the Na-D fluorescence. The molecular transition states for the different energy levels are labeled by $[Na \cdots I]^{\ddagger *}$ and $[Na \cdots I]^{\ddagger **}$. The right panels show the intensity of the Na-D fluorescence signal as function of the delay time between pump and probe laser pulses. The molecular motion within the adiabatic potential range is reflected by an oscillatory signal. The tunneling at the crossing point results in a steady decay of the oscillation amplitudes (top right). On the other hand, this periodic transition onto the diabatic repulsive potential branch results in a step-wise increase of the product signal (bottom right).*

The probe excitation transfers the molecule into a further transition state $[\mathrm{Na} \cdots \mathrm{I}]^{\ddagger **}$, which dissociates without further barrier. The observed transient signal is determined by the periodic motion of the wave packet and thus reflects the vibrational motion of the excited NaI^* molecule. The partial transmissivity of the potential barrier at the avoided crossing results in a periodic decrease of the signal intensity, which is directly correlated to a stepwise increase of the fluorescence intensity observed with a probe wavelength of 589 nm (λ_{pr}^{∞}, see lower right panel). This probe pulse is in resonance with the Na-D transition of sodium and therefore reflects the amount of product formed by the dissociation resulting from the tunneling through the avoided crossing.

The two-pulse pump-probe spectroscopy is not only limited to probe steps exciting fluorescence. There are many different possibilities, which all follow similar schemes. In all cases the two requirements, temporal and energetic (spatial coordinate + energy states involved) selectivity have to be achieved. Examples are (i) ion-detection, (ii) transient absorption spectroscopy, (iii) linear anti-Stokes Raman spectroscopy, etc. Just some few remarks concerning the three methods mentioned:

(i) The ion-detection makes use of transitions above the ionization limit of molecules. After ionization the ions but also the photo electrons can be detected. For the ions, mass spectroscopic techniques offer high sensitivity and in addition information about products when *e.g.* different molecular fragments result. The main restriction of this technique is the fact that vacuum conditions are required for the ion or electron detection. Typically, molecular beam arrangements are used in combination with mass or photo electron spectrometry.

(ii) Transient absorption spectroscopy is a widely used and powerful technique. Here, the absorption of the probe laser light as a function of the time delay between pump and probe laser pulses is measured. The probe laser can be in resonance with electronic (mostly in the visible or UV spectral region) or vibrational or rotational energy levels (IR light). Since the pump laser pulse excites the molecules into higher energy states, also these states are available for absorption processes. The probe wavelength can be set to a specific transition in the molecule or it can be varied to obtain a full transient absorption spectrum. In the latter case for more efficiency broadened laser pulses ("white light continuum") are used to take complete absorption spectra without scanning the probe laser wavelength. A major difficulty with this technique is the fact that different states may contribute, which absorb but also emit light. This means that the experimenter has to very carefully analyze the various negative and positive contributions to the transient transmission spectrum.

(iii) Raman spectroscopy, named after the Indian physicist Sir Chandrasekhar V. Raman (1888–1970, Nobel Prize in Physics 1930), is based on the inelastic scattering of photons from molecules (for an energy scheme, see Fig. 5). Due to the interaction of the scattered photons with the molecules, these molecules can gain some energy, which on the other hand is lost by the photons. Thus, this red shift ("Stokes-shift") of the light

reflects internal energies (let us consider *e.g.* vibrational energies) of the molecule and therefore can be used in frequency-domain spectroscopy to investigate the vibrational mode energies. In time domain, a second Raman process induced by the time-delayed probe laser can now be used to study relaxation processes of the vibrational levels, which were populated by the first (pump-induced) Raman process. At low temperatures these excited energy levels in most cases are not populated ("Boltzmann distribution") without the pump interaction. Since for the second scattering process a number of molecules with excited vibrational modes are present, the inelastically scattered photons also can gain energy, leaving the molecules in their vibrational ground state after the scattering process. The now also observed blue shift ("anti-Stokes shift") of the scattered light measures the amount of excited molecules as a function of time delay between pump and probe laser pulses and of the considered mode energy. This time-resolved Raman technique allows for the investigation of vibrational or rotational mode dynamics in the electronic ground state. Unfortunately, compared to the elastic scattering ("Rayleigh scattering"), Raman scattering is a very weak process yielding only little signal intensity. Due to this the technique is difficult to use and required very sensitive detection.

In order to overcome some of the limitations of the standard two-pulse pump-probe spectroscopy, in the following section an alternative approach is discussed, which is based on the nonlinear interaction with several laser pulses for both pump and probe steps.

3.2 Four-Wave Mixing Spectroscopy — Example: CARS

While the Raman scattering shortly discussed above is a linear process, *i.e.* the resulting signal (for moderate laser powers, where saturation effects do not play a role) depends linearly on the power of the incoming laser, there are also processes, where the signal depends on more light fields. The source of the signal radiation is the polarization P. While in everyday life processes play a role, where P is directly proportional to the light field E, for the general case also a nonlinear dependence on higher orders has to be taken into account:

$$P = \varepsilon_0 \left\{ \chi^{(1)} E + \frac{1}{2!}\chi^{(2)} EE + \frac{1}{3!}\chi^{(3)} EEE + \ldots \right\} = P_L^{(1)} + P_{NL}^{(2)} + P_{NL}^{(3)} + \ldots \tag{9}$$

In this rather simplified relation, $P_L^{(1)}$ is the linear polarization while the $P_{NL}^{(i)}$ are the nonlinear contributions of i^{th} order. $\chi^{(i)}$ are the respective susceptibility tensors. The product of light field amplitudes (*e.g.* EE) can also involve fields of different light sources, having different wavelengths, pulse envelopes, etc. A simple case would for example be the frequency doubling, which would be described by

$$P_{NL}^{(2)}(2\nu) = \frac{1}{2!}\chi^{(2)} E(\nu) E(\nu)\,. \tag{10}$$

Very useful for femtosecond time-resolved spectroscopy are four-wave mixing (FWM) processes where three laser pulses interact with the system to generate a fourth light field. According to Equ. 9, this process is described by the nonlinear susceptibility $\chi^{(3)}$. Due to the involvement of several lasers different FWM schemes are possible, like *e.g.* degenerate FWM (DFWM) where all fields have the same wavelength. In the following we will concentrate on a nonlinear Raman approach, "coherent anti-Stokes Raman scattering" (CARS).

The CARS technique is illustrated in Fig. 5. The energy scheme shown on the left side is identical to the energy scheme, which would have to be drawn for the linear anti-Stokes Raman method described above. However, there is an important difference. While in the linear case, the arrow marked by ν_S would be the spontaneous, Stokes-shifted Raman scattering signal of the first laser interaction (ν_{pu}), for CARS ν_S represents a laser pulse at the Stokes frequency. Both pump and Stokes laser coherently excite molecular vibrations (or also rotations, electronic states) when their energy difference equals the respective mode energy. The third laser, here called probe laser, is scattered coherently from this concerted motion of molecules and results in a signal at a frequency ν_{aS}, which is anti-Stokes shifted by the frequency of the excited vibrational mode. The frequency of the probe laser, ν_{pr}, may be different from the other laser frequencies. Very often $\nu_{pr} = \nu_{pu}$ is chosen for simplicity. The nonlinear polarization for the CARS process is given by

$$P^{(3)}(\nu_{aS}) = \varepsilon_0 \frac{1}{3!} \chi^{(3)} E_{pu}(\nu_{pu}) E_S^*(\nu_S) E_{pr}(\nu_{pr})\,. \tag{11}$$

Looking to the scheme, it becomes obvious that the energy conservation is fulfilled by the photons, *i.e.* no energy is transferred from or to the molecule:

$$h\nu_{aS} = h\nu_{pr} + (h\nu_{pu} - h\nu_S) = h\nu_{pr} + h\nu_R\,, \tag{12}$$

where ν_R is the frequency of the Raman mode. A further, very important condition results:

$$\vec{k}_{aS} = \vec{k}_{pr} + (\vec{k}_{pu} - \vec{k}_S) = \vec{k}_{pr} + \vec{k}_R\,. \tag{13}$$

This relation represents the momentum conservation where again the molecule, which remains in its original state after the CARS interaction, does not contribute. As a consequence, the geometry of the nonlinear interaction is not arbitrary. Strong signals only result when the "phase matching conditions" are fulfilled. While the spontaneous Raman signal is scattered into all directions, the anti-Stokes signal of the CARS process is a collimated beam along a fixed direction, which is determined by the laser beam arrangement as well as the dispersion of the medium. Due to the latter, the lengths of the wave vectors are not equal multiples of the frequencies, but depend on the indices of refraction for the given wavelengths:

$$k_i = |\vec{k}_i| = \frac{2\pi\nu_i n_i}{c_0}\,, \tag{14}$$

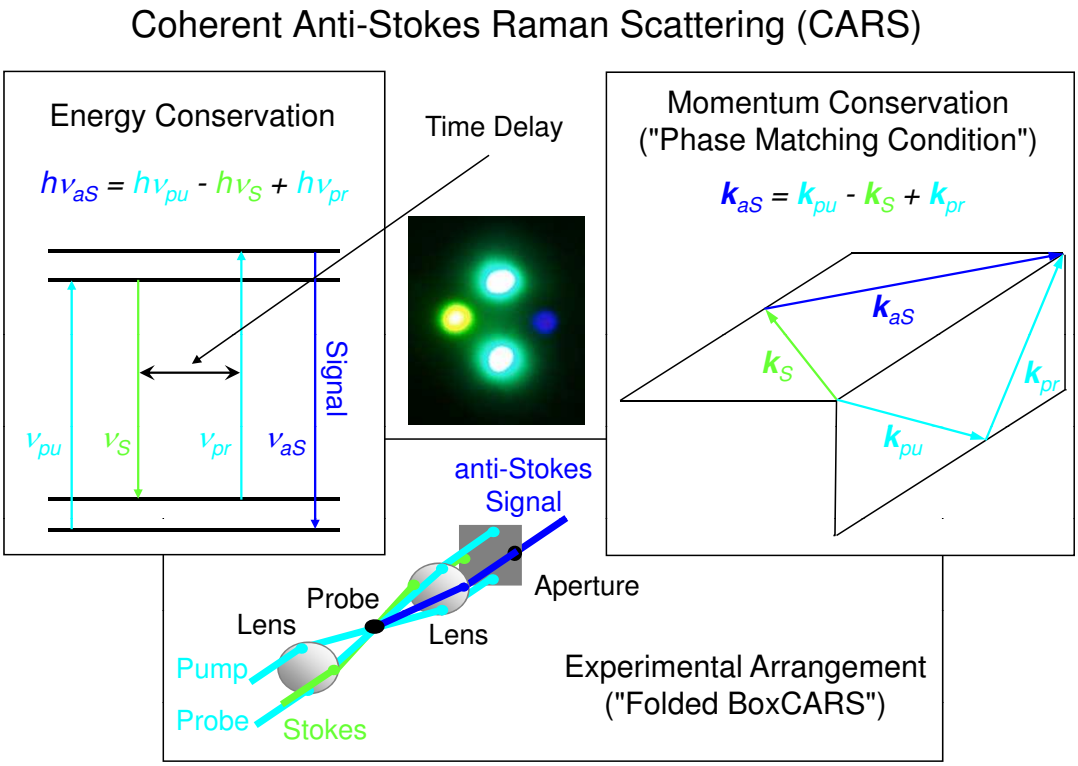

Figure 5: *Laser light is scattered from molecules into all directions. Next to the most intense spontaneous scattering part ("Rayleigh scattering") also a weak inelastic "Raman scattering" can be observed. Here, usually light at lower energies compared to the energy of the incoming laser photon is detected. The red shift ("Stokes shift") is due to the excitation of e.g. vibrational modes of the scattering molecules and thus is equal in energy to these molecular energies. The spontaneous Stokes Raman process populates excited vibrational states and therefore can be considered to be a pump step with excitation frequency ν_{pu} (see energy level diagram in the left panel). The dynamics of the vibrational states would in a two-pulse anti-Stokes Raman experiment be measured by the interaction of a time-delayed probe laser at ν_{pr}, which results in a blue shifted ("anti-Stokes shift") signal as long as the excited vibration states are populated. In the coherent anti-Stokes Raman scattering (CARS) two laser pulses (pump at ν_{pu} and Stokes at ν_S) coherently excite the vibrational mode with frequency ν_R if $\nu_{pu} - \nu_S = \nu_R$. The molecules oscillating in common mode now interact with a third laser pulse, the probe laser at ν_{pr} and generate a coherent signal at the anti-Stokes shifted frequency ν_{aS}. Thus, the energy is conserved within the photons. The molecule after the CARS interaction remains in its original state. Due to the conservation of the momentum, the phases of the laser and signal light has to be matched. A possible "phase matching arrangement" is depicted in the right panel. At the bottom the experimental setup of this "folded BoxCARS" geometry is shown. The resulting anti-Stokes signal is collimated and can be very intense as can be seen in the photo taken from the lasers and signals on a screen placed in front of the aperture shown in the drawing below.*

where c_0 is the vacuum speed of light. For the fulfillment of the phase matching condition different geometries are possible. In Fig. 5 the "folded BoxCARS" arrangement is shown (vector diagram in top right panel, experimental setup in bottom panel), which is ideal for time-resolved experiments, since laser pulses and signal are spatially well separated. The photo in the center of Fig. 5 was taken from the signal together with the laser pulses behind a cuvette filled with benzene. The Raman excitation was resonant with the fully symmetric breathing motion of the benzene ring.

One detail, which hardly is discussed in any textbook should be pointed out here. In Equ. 13, a wave vector $\vec{k}_R$ is introduced. This vector can be assigned to the generated and afterwards destroyed vibration (phonon) of the molecular system. For isotropic media, this vector does not have too much importance. However, when investigating *e.g.* crystals, the orientation of $\vec{k}_R$ has to match the direction of the phonon vector of interest. In ref. 11 femtosecond CARS experiments are described on single crystals of polydiacetylenes. In these crystals all the linear polymer chains are oriented parallel to one of the crystal axes. To perform CARS spectroscopy on the chain modes, making also use of a resonant excitation (*i.e.* using laser wavelengths in resonance with the absorption of the conjugated π electrons along the polymer backbone) is only possible if $\vec{k}_R$ is oriented parallel to the polymer chains.

3.3 Four-Wave Mixing Spectroscopy — The Degrees of Freedom

As was already mentioned above, four-wave mixing (FWM) spectroscopy is a rather flexible tool due to the use of more laser fields compared to the two-pulse pump-probe technique. Many degrees of freedom are available, which help to adapt the method to the system under investigation. The degrees of freedom listed in the following can be combined to obtain "multi-dimensional" information.

- **Laser Wavelength** — The laser wavelength can be tuned to meet resonance conditions. Electronic resonances with higher lying absorption states on the one hand drastically enhance the signal, on the other hand also dynamics of the excited state becomes accessible. The difference between the wavelengths of the lasers is used to resonantly excite *e.g.* vibration modes, but it also decides what kind of spectroscopy is performed. As will be discussed below, next to CARS there are many other FWM processes like degenerate FWM (DFWM), transient grating spectroscopy, etc.

- **Timing** — Of course in time-resolved spectroscopy the timing of the lasers is decisive. As will be shown below, depending on the technique applied, information about different dynamics can be obtained, like vibrational dynamics in different electronic states and different relaxation processes can be measured like coherence or population life times.

- **Signal Spectrum** — The spectrum of the signal (*e.g.* anti-Stokes Raman) is not highly resolved since the femtosecond lasers used are spectrally broad. Nevertheless,

assignments to different vibrational modes are possible in many cases. For these modes dynamics and interaction with other modes can be studied. The signal wavelength at which the transient is observed as a function of delay time between contributing lasers in some cases also determines what kind of information can be seen as will be demonstrated below.

- **Beam Geometry** — Even for a given set of pulse wavelengths completely different processes can take place when the geometry of the beam arrangement is changed. Thus, a CARS experiment measuring the vibrational coherence easily can be converted into a population grating experiment where T_1 times of electronic states are measured.

- **Signal Dynamics** — The signal itself also shows dynamics, which can be measured by using a heterodyne technique where the signal is mixed with a reference field (local oscillator). By this, the signal can be temporally resolved (scanning the reference pulse over the signal pulse), but it can also be enhanced.

- **Light Polarization** — As is well known from frequency resolved spectroscopy, light polarization can be used to selectively excite molecular modes according to symmetry selection rules. Additionally, in femtosecond time-resolved spectroscopy the combination of different polarizations is used to *e.g.* suppress signal contributions due to rotational motion ("magic angle"), to suppress non-resonant back ground signals (*e.g.* CARS signal of solvent), etc.

- **Pulse Shape** — Instead of using Fourier transform limited laser pulses also chirped pulses (the different spectral parts of the laser pulse are linearly or nonlinearly arranged along the time coordinate) can be used for FWM spectroscopy. Thus, molecular dynamics can be influenced and spectral features suppressed or enhanced.

We will now discuss some examples for possible (not all) variations of the FWM process. For this, we will consider another simple molecule, iodine (I_2) in the gas phase. Figure 6 shows the potential energy scheme of iodine together with example transitions used in two-pulse pump-probe spectroscopy. The pump laser pulse prepares a wave packet on the electronically excited B state. The B state is a bound state. Therefore, an oscillating wave packet results, which is probed by the probe laser interaction resulting in fluorescence from the ion-pair states of the molecule. A typical transient is depicted in the right panel. Due to the use of a "magic-angle" between the pump and probe laser polarizations of approximately 54.7° the modulation of the signal caused by molecular rotations is omitted. The fast oscillation is due to the periodic motion of the wave packet and reflects the molecular vibration. The slow modulation is due to dephasing and rephasing, which originates from the formation of the wave packet from overtones having different spacings in the anharmonic potential.

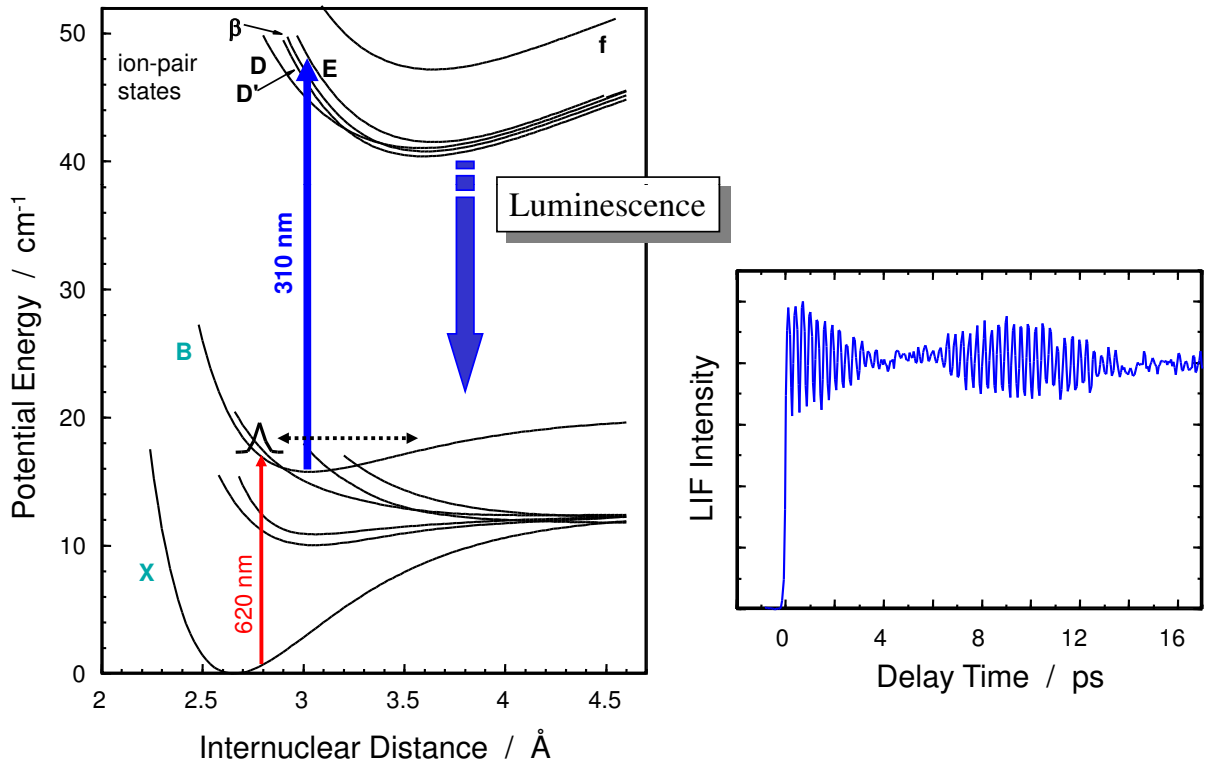

Figure 6: *On the left, the potential energy diagram of iodine is depicted. The arrows indicate transitions used for a two-pulse pump-probe experiment. The probe interaction is detected via the fluorescence from the ion-pair states. The signal is plotted as a function of delay time between pump and probe laser pulses on the right side. Here, the oscillatory motion of the wave packet as well as the modulation due to the superposition of overtones with different level spacing can be clearly seen. The slow dephasing and rephasing would not occur if the B potential would be harmonic.*

3.3.1 The timing of the laser pulses

For the FWM experiments, we assume that three laser fields interact with the ensemble of I_2 molecules in a folded BoxCARS arrangement as mentioned above. In all experiments two laser pulses are coincident in time, while the third pulse arrives with a variable time delay Δt. Depending on the relative timing of the three laser pulses, different dynamics in the molecules are probed by one or two photon interactions resulting in the coherent FWM signal. The FWM techniques applied to the investigation of the molecular dynamics in gaseous I_2 are

- coherent anti–Stokes Raman scattering (CARS),
- coherent Stokes Raman scattering (CSRS),

- and degenerate four-wave mixing spectroscopy (DFWM).

In the femtosecond CARS experiment, two laser pulses (pu and pu_τ; the name "probe" was deliberately avoided to avoid confusion) have the same wavelength, $\lambda_{pu} = \lambda_{pu_\tau}$. The third laser pulse (S) is tuned to a lower wavelength λ_S in such a way that the difference between pu and S laser wavelengths is resonant with a vibrational Raman transition in the iodine molecule. While one of the pump pulses (pu) and the Stokes pulse S are coincident in time, the second pump pulse pu_τ arrives with a variable delay time. Figure 7 shows the experimentally observed CARS intensity as a function of delay time Δt between the pump pulse pu_τ and the two time coincident pulses pu and S for I_2 vapor. The transient was obtained for a pump wavelength $\lambda_{pu} = \lambda_{pu_\tau} = 620$ nm and a Stokes wavelength $\lambda_S = 645$ nm detecting the coherent anti–Stokes signal at $\lambda_{aS} = 596$ nm. For negative delay times ($\Delta t < 0$) of pu_τ, the transient is characterized by beats with a period of approximately 300 fs, which corresponds to an energy difference of 111 cm^{-1}. This value agrees with the energy spacing found between the vibrational eigenstates of iodine in the excited B state, which are reached by the $\lambda_{pu_\tau} = 620$ nm laser pulse from the ground state. For positive delay times ($\Delta t > 0$) the signal shows oscillations at about twice the frequency of the oscillations at negative delay times ($\Delta t < 0$). These short time oscillations for $\Delta t > 0$ show a period of 160 fs, corresponding to the wave packet motion prepared by coherent two photon pumping (pu and S) around the third vibrational level in the ground X state of iodine, because the wavelength difference between pu and S laser was tuned to the second overtone ($\Delta v'' = 3$) of the I_2 ground state vibration. The average period of the oscillations corresponds to a vibrational wavenumber spacing of about 208 cm^{-1}. This agrees with the vibrational energy spacing in the ground X state of iodine around $v'' = 3$ as observed from continuum resonance Raman experiments [12].

This means that femtosecond time-resolved CARS depending on the timing of the laser pulses gives information about vibrational dynamics in different electronic states. In contrary to the two-pulse pump-probe experiment no fluorescing state (or ionization or similar) is required to obtain the data.

3.3.2 The wavelengths of the laser pulses

Now, changing the laser wavelengths does not only result in different resonances, but also different FWM processes result. The DFWM transient discussed in the following was recorded using three laser fields having the same central wavelength λ_0, which is resonant with discrete rot–vib eigenstates in the excited B state of iodine. While two laser pulses (pu_1 and pu_2) are coincident in time, the third pulse (pu_τ) arrives with a variable time delay. Panel (A) of Fig. 8 (in panel (B), a CARS transient is given again for comparison) shows a typical DFWM transient of iodine as a function of the delay time Δt between the variable laser pulse, pu_τ, and the fixed, simultaneous laser pulses pu_1 and pu_2. The transient exhibits well defined 300 fs beats, corresponding to a vibrational energy spacing of about 111 cm^{-1}. This agrees

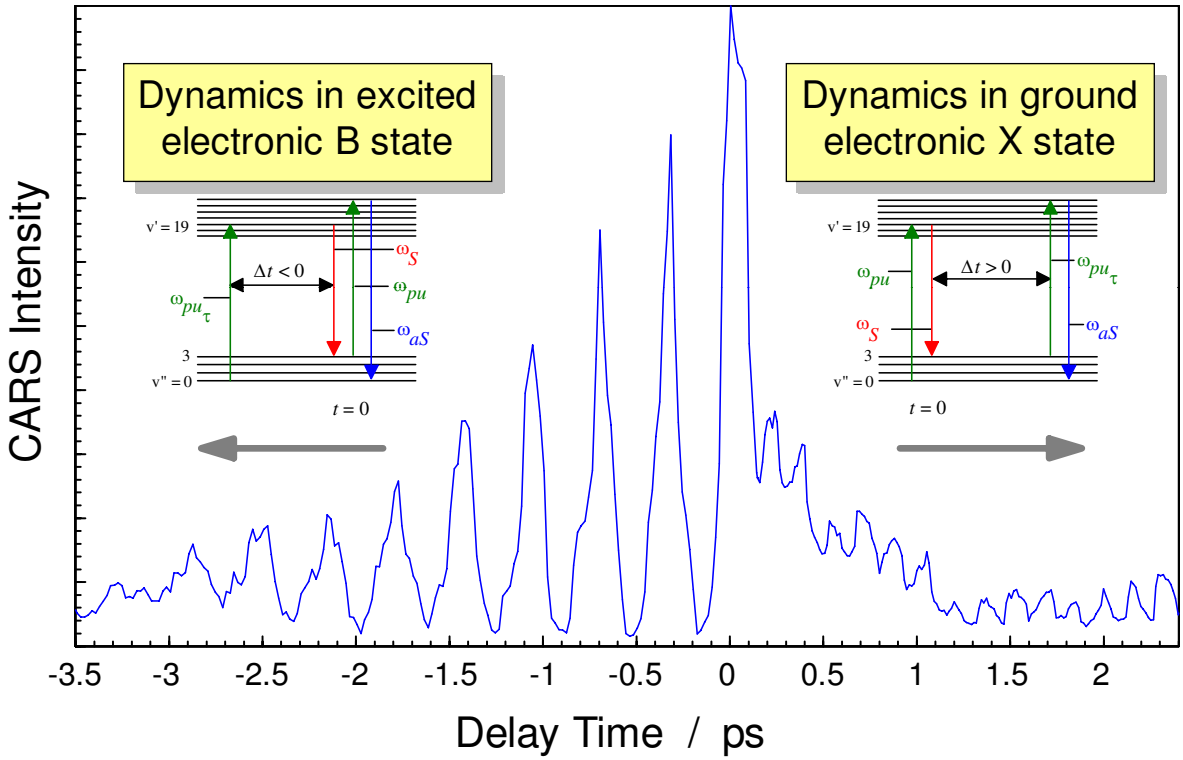

Figure 7: *The effect of timing the laser pulses shown for CARS on iodine. Depending on the time sequence of the laser pulses the vibrational dynamics either in the electronic excited or ground state are probed. The periodic behavior of the transient CARS signal can be converted into frequency domain information by performing a Fourier transform, which gives the beating frequencies of the vibrational states involved. For iodine these beating frequencies are the frequency differences between the excited overtones.*

well with the experimental vibrational energy spacings in the excited B state of gaseous iodine accessed by the 620 nm lasers. For positive delay times ($\Delta t > 0$) additional beats having about twice this wavenumber appear. These oscillations show a period of 155 fs, which corresponds to an energy spacing of 215 cm^{-1} and reflects the dynamics of a wave packet within the electronic ground state of iodine.

A femtosecond CSRS transient is displayed in panel (C) of Fig. 8. Here, the signal is Stokes shifted. The transient shows a completely different time behavior than that found for DFWM [panel (A)] or CARS [panel (B)]. In the CSRS experiment also three laser fields interact with the ensemble of I_2 molecules. Two laser pulses have the same wavelength, $\lambda_{pu} = \lambda_{pu_\tau}$, and below will be referred to as pump lasers in consistency with the CARS experiment. In contrast to the CARS experiment, the third laser (anti-Stokes) is tuned to a lower wavelength, λ_{aS}, such that the difference between pump and anti–Stokes laser wavelength is resonant with a vibrational transition in the ground state. Panel (C) of Fig. 8 shows the CSRS transient

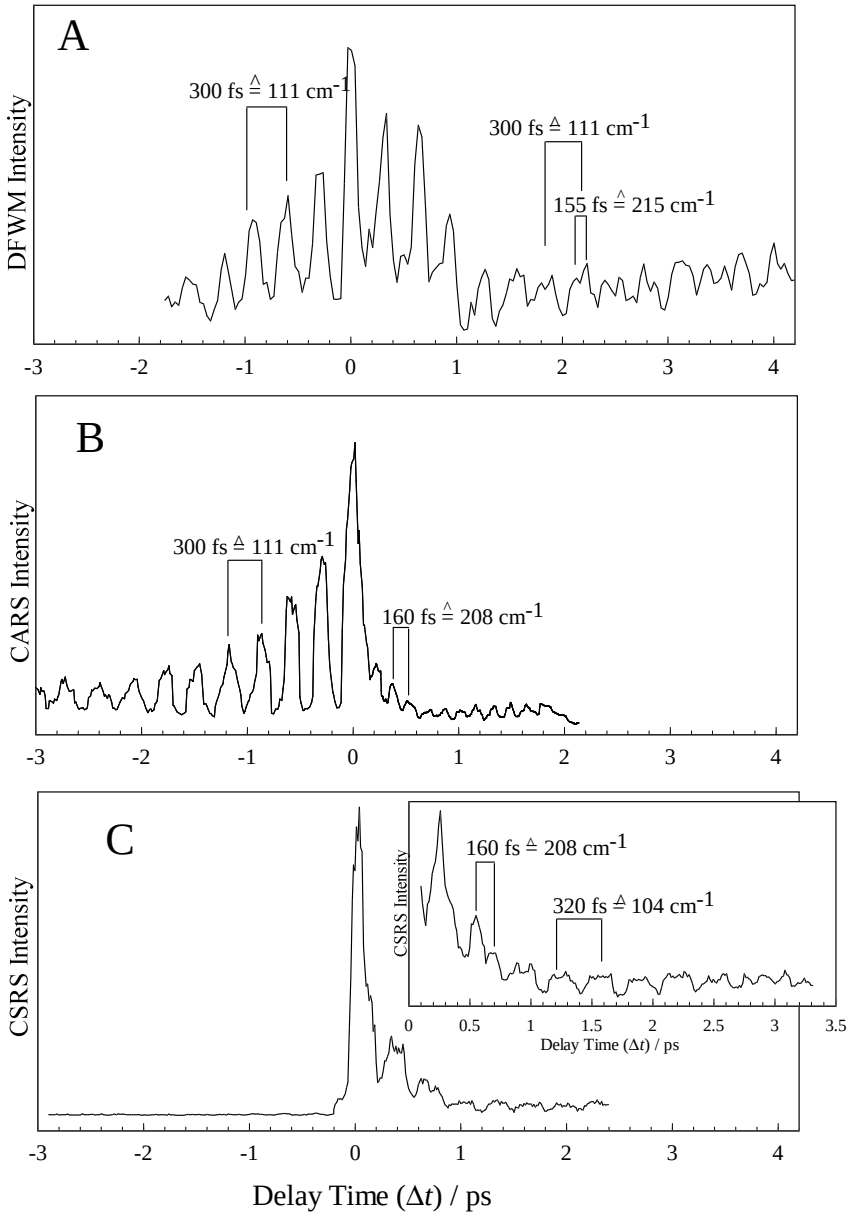

Figure 8: *Femtosecond FWM transients of gaseous iodine: (A) fs–DFWM transient ($\lambda_{pu_1} = \lambda_{pu_2} = \lambda_{pu_\tau} = \lambda_{DFWM} = 620$ nm). (B) fs–CARS transient ($\lambda_{pu} = \lambda_{pu_\tau} = 620$ nm, $\lambda_S = 645$ nm, $\lambda_{aS} = 596$ nm). (C) fs–CSRS transient ($\lambda_{pu} = \lambda_{pu_\tau} = 615$ nm, $\lambda_{aS} = 591$ nm, $\lambda_S = 641$ nm).*

as a function of the delay time Δt between the pulse pu_τ and the two time coincident pulses pu and aS. For a pump wavelength $\lambda_{pu} = \lambda_{pu_\tau} = 615$ nm and an anti–Stokes wavelength $\lambda_{aS} = 591$ nm the coherent Stokes signal is detected at $\lambda_S = 641$ nm. As it is the case for the CARS transient also here the wavelengths of the pump lasers pu and pu_τ determine where the interaction with the excited state potential takes place. The difference of the wavelengths between pump (pu) and anti–Stokes (aS) laser ($\lambda_{aS} - \lambda_{pu}$), which was chosen to be resonant with the second overtone $\Delta v'' = 3$ within the ground state of the iodine molecules, gives the position accessed in the ground state potential. The transient shows neither a signal nor a beating structure for negative delay times ($\Delta t < 0$). For positive delay times ($\Delta t > 0$) the transient exhibits well defined 320 fs beats, corresponding to a vibrational energy spacing of about 104 cm^{-1}. This agrees well with the experimental vibrational energy spacings in the excited B state of gaseous iodine accessed by the 615 nm pump lasers. Also beats having about twice this wavenumber appear. These can be assigned to the electronic ground state. The FFT spectrum of the CSRS transient (not shown) also exhibits two distinct components at 111 and 208 cm^{-1}. The peak at 111 cm^{-1} can be assigned to the vibrational coherences in the B state of iodine, while the peak at 208 cm^{-1} corresponds to the second overtone ($\Delta v'' = 3$) of iodine in the electronic ground state. That is exactly what could be expected from the experimental conditions as mentioned above.

3.3.3 Some "qualitative" theory

Theory helps to understand the dependence of the observed dynamics on the timing of the laser pulses as well as the variation of the laser wavelengths resulting in the different FWM techniques. The nonlinear polarization responsible for the FWM signal can be theoretically described using density matrix formalism. An elegant method for calculating the elements of the involved density matrix is using time-evolution energy ladder diagrams according to Albrecht *et al.* [13, 14] (for the formalism associated with these time–evolution diagrams see refs. 13 and 14). These diagrams include a time ordering of the possible interactions as well as information about the interactions themselves. The nonlinear susceptibility or polarization is derived by summing up all possible diagrams. If spectroscopical results in the frequency domain are described by this technique, a selection of important diagrams can be performed on the basis of resonance conditions. This means that the choice of laser frequencies (different FWM techniques) together with the molecular transition determine which diagrams are of importance and which are not. For the femtosecond time resolved experiments on systems, which show coherences much longer than the pulse durations (as is the case for iodine vapor used in the above described experiments) the timing of the laser pulses additionally selects diagrams, which have the right time ordering.

Figure 9 shows the time–evolution diagrams that illustrate the contribution for the three FWM processes (DFWM, CARS, CSRS) for negative [diagrams (A) and (B)] and positive [diagrams (C)–(E)] delay times. For simplicity, we neglect in our discussion diagrams starting with transitions from thermally occupied higher vibrational ground state levels. With the help of these diagrams, one can determine in what electronic state (ground state or B state)

the wave packet is generated by the laser pulse(s) that interact(s) with the system first. From this, one can easily conclude whether the dynamics of the electronic ground or the B state are monitored by the time dependent FWM signal.

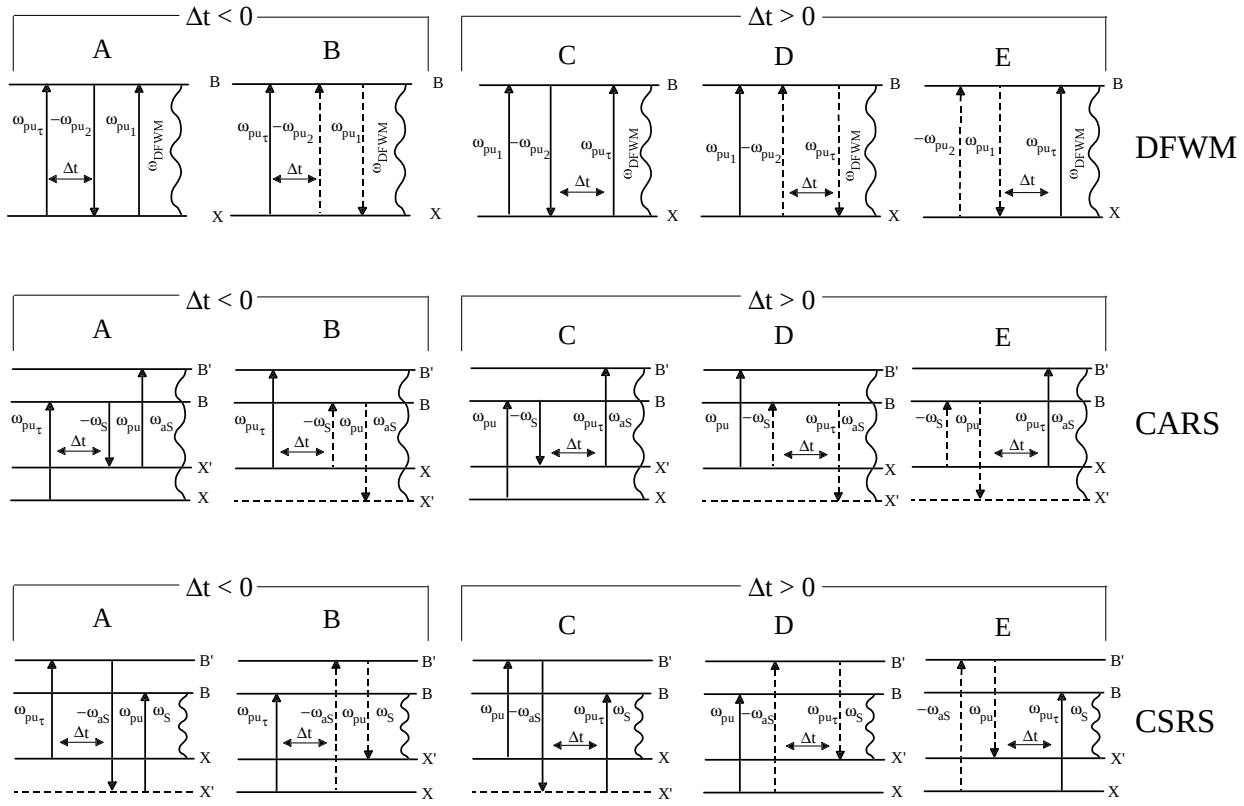

Figure 9: *Relevant time-evolution diagrams describing the femtosecond time-resolved FWM processes DFWM, CARS and CSRS for $\Delta t < 0$ [diagrams (A) and (B)] and $\Delta t > 0$ [diagrams (C)–(E)]. The solid and dashed arrows represent a ket and a bra side transition, respectively. See Refs. 13 and 14 for details.*

In the case of the femtosecond time-resolved DFWM process pu_τ prepares for negative delay times ($\Delta t < 0$) a wave packet in the B state. Therefore, the time dependent DFWM signal reflects the dynamics of the excited B state. This is characterized by diagrams (A) and (B). For positive delay times ($\Delta t > 0$), a superposition of the ground and B state dynamics can be observed in the resulting DFWM transient signal. This corresponds to diagrams (C)–(E), which demonstrate the preparation and subsequent DFWM signal of vibrational coherences in the ground state as well as the excited B state. Diagrams (C) and (E) illustrate the motion of a wave packet in the electronic ground state. This wave packet is prepared by the laser pulses pu_1 and pu_2, which interact simultaneously with the iodine molecules. On the other hand, diagram (D) illustrates the dynamics of a wave packet in the excited B state, which is prepared by an excitation similar to a "two–photon" absorption by pu_1 and pu_2. The quantitative contribution of each diagram to the total DFWM signal can only be determined

by means of quantum mechanical calculations. Quantum mechanical calculations by Meyer *et al.* [15] based on these diagrams show excellent agreement between the experimental and the calculated transients.

The situation is more complicated for the coherent Raman techniques CARS and CSRS due to the non–degeneracy of the laser and signal wavelengths. The diagrams (A) and (B) corresponding to the CARS process for negative delay times ($\Delta t < 0$) reflect the dynamics of a wave packet prepared by pu_τ in the B state of iodine. The main contribution to the transient CARS signal for $\Delta t < 0$ is given by diagram (A) because, in contrast to diagram (A), diagram (B) shows no Raman resonance. If positive delay times ($\Delta t > 0$) are chosen both pu and S excite the molecules, which afterwards are probed by pu_τ. Diagram (C) and (E) are reflecting the ground state dynamics in the CARS signal, while diagram (D) illustrates the motion of a wave packet in the B state. However mainly diagram (C) will contribute to the CARS signal for positive delay times due to the missing Raman resonance in the diagrams (D) and (E). Therefore, the fs–CARS signal for $\Delta t < 0$ is mainly determined by diagram (A) and for $\Delta t > 0$ diagram (C) is playing the main role. This is in excellent agreement with the experimental CARS transient (panel (B) of Fig. 8) where for negative delay times ($\Delta t < 0$) the wave packet dynamics in the B state [diagram (A)] and for positive delay time the ground state dynamics [diagram (C)] of iodine can be resolved (For quantum mechanical calculations by Meyer *et al.* see ref. 16).

The time dependent CSRS signal should for negative delay times ($\Delta t < 0$) reflect the dynamics of the excited B state. This is characterized by diagrams (A) and (B), where diagram (B) plays the main role because of the missing Raman resonance in diagram (A). For positive delay times the diagrams (C) and (E) illustrate the motion of a wave packet in the electronic ground state, which was prepared by the simultaneous interaction with pu and aS. Again, diagram (C) will play a minor role, due to the fact that it shows no Raman resonance. On the other hand diagram (D) illustrates the dynamics of a wave packet in the excited B state, which is prepared by an excitation similar to a two photon absorption by pu and aS. From this, the CSRS transient should reflect the dynamics of the B state for $\Delta t < 0$ [diagram (B)] and for $\Delta t > 0$ a superposition of the ground [diagram (E)] and B state [diagram (D)] dynamics should be observed in the resulting CSRS transient signal. The assumption for positive delay times ($\Delta t > 0$) is consistent with the experimental results [panel (C) of Fig. 8). However, for negative delay times ($\Delta t < 0$) no signal at all could be observed in the experimental transient. So the influence of diagram (B) in comparison to the diagrams (D) and (E) seems to be negligible.

3.3.4 The signal spectrum

We have seen in the last subsections that by choosing different wavelength contributions also different FWM techniques are selected. However, one always should keep in mind that *e.g.* when detecting a DFWM signal complete information only can be gained if the full spectrum is analyzed as a function of laser delay times. This is demonstrated for a DFWM experiment

on gaseous iodine. Taking the full spectrum as a function of delay time between the two laser pulses (pu_1 and pu_2), which are coincident in time, and the third pulse (pu_τ) yields an intensity plot as a function of two variables, the detection wavelength and the delay time.

An analysis of the different dynamics of the FWM signal with the help of cross-sections made through the multi-dimensional plot along the time axis at different detection wavelengths shows that there are three characteristic contributions within the spectral components of the signal pulse. These three distinct contributions are displayed in Fig. 10 and show themselves at the central wavelength of the pulse at $\lambda_{det} = 572.4$ nm (lower panel), blue shifted from the central wavelength at 566.6 nm (middle panel) and shifted to the red side of the pulse at 578.9 nm (upper panel). Generally, this change in the behavior of the signal with respect to the detection wavelength can be attributed to the polychromatic nature of the broadband femtosecond laser pulses employed. The different wavelengths incorporated in these laser pulses allow for three different FWM processes, CARS, DFWM, and CSRS to occur simultaneously. These processes show themselves at different wavelengths of the broadband signal. An analysis of the results yields exactly the same mode contributions for the different timings as we already have discussed above.

3.4 Experiments on Complex Systems

While up to now we have considered rather simple systems like sodium iodide or iodine (which are complicated enough if one goes into details ...), in the following a more complex system will be considered. Especially for bigger molecules, where many different vibrational modes and electronic states exist and partially couple, advanced spectroscopic techniques are required.

3.4.1 Our example — carotenoids

Since the first experiments in femtochemistry, fast progress has been made. In the meantime also complex dynamics like proton transfer, ring-opening, *cis-trans* isomerization, and other processes have been analyzed by means of femtosecond time-resolved spectroscopy (see for example ref. 17). More advanced measuring techniques allow for a more and more detailed insight into such dynamics. Exceptionally demanding are experiments on biologically relevant systems.

The light-driven reactions responsible for photosynthesis in nature are responsible for the conversion of sunlight energy into chemical energy. For this, the light energy is absorbed by antenna complexes. From there an energy transport chain finally transfers the energy into the reaction center where the energy conversion takes place. Embedded into a protein matrix different pigment molecules work together for the light absorption. In Fig. 11, *e.g.* the pigment molecules of the peripheric antenna system ("light harvesting system II") of the purple bacteria *rhodopseudomonas acidophila* are displayed.

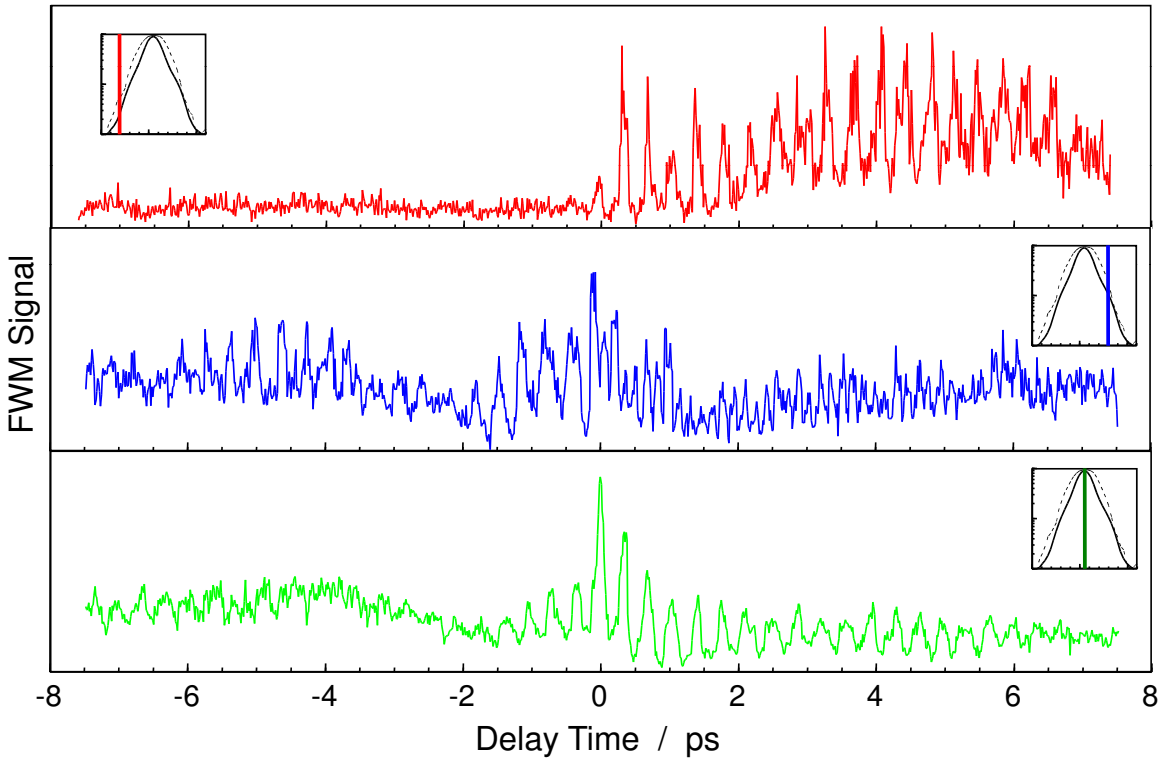

Figure 10: *The result of a femtosecond time-resolved DFWM experiment on gaseous iodine when detected at different spectral positions of the signal. The lower panel shows the transient detected at the center position of the spectrum as one usually would do for a DFWM scheme. A typical DFWM transient results as already discussed earlier. However, when the detection wavelength is shifted to the anti-Stokes (middle panel) or Stokes (top panel) side of the spectrum transients can be found, which show the dynamics expected for a CARS or CSRS experiment, respectively.*

The carotenoid chains are depicted as turquoise molecules while the chlorophyll molecules are yellow and red, representing different absorption spectra due to differing environment. To understand the function of this complex system, intra and intermolecular energy transport has to be analyzed in detail. These processes are very efficient and take place on a time scale of femtoseconds to picoseconds. With the help of femtosecond time-resolved experiments the transfer of energy from carotenoid to chlorophyll molecules has been successfully studied [18]. Here, internal, radiationless processes within the carotenoid molecules can drastically reduce the efficiency. Nature accomplishes an optimization of the intermolecular energy flow while at the same time minimizing the intramolecular loss channels. The latter are strongly coupled to molecular vibration modes.

In Fig. 12 typical intramolecular processes are indicated like they can also be found in carotenoids after light absorption. Here, on a femtosecond time scale in most cases only

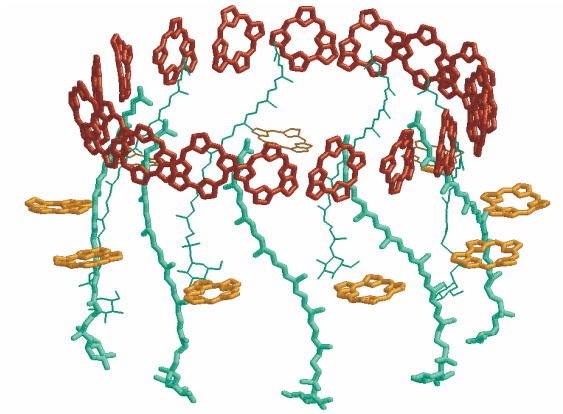

Figure 11: *An important step during photosynthesis is the absorption of sunlight and the following transport of the energy within the photosystem of the plant or – as in the present example – bacteria. Responsible for this are pigment molecules. In the peripheric antenna complex of the purple bacteria rhodopseudomonas acidophila carotenoid and chlorophyll molecules interact. The scheme shows these pigment molecules extracted from the complex matrix system. The different molecules provide the absorption of light at different parts of the light spectrum. Here, the carotenoids (turquoise) transfer their energy to the chlorophyll molecules (yellow and red), from where finally the reaction center is energized. The intra and intermolecular energy transport can be investigated by femtosecond time-resolved spectroscopy. [By courtesy of J. Herek, Amsterdam]*

singlet states (multiplicity $(2S + 1) = 1$) are of relevance. In carotenoids the absorption takes place due to a transition between the ground state S_0 and the excited state S_2. The lower-energetic state S_1 is a "dark state", *i.e.* due to symmetry rules the transition $S_1 \leftarrow S_0$ is forbidden. Nevertheless, population is also transferred into S_1 via a radiationless internal conversion (IC), which is coupled to a vibration mode of the molecule. During this process, excited vibration states (hot states) of the S_1 state are populated. Besides this, also other electronic states might be involved in the transfer process, which is still under discussion and therefore an interesting task for future experiments. Now, different processes play a role for the further dynamics. On the one hand, collisions with the surroundings ("bath") can result in a cooling ("vibrational relaxation", VR) of the molecule. On the other hand, a fast redistribution of vibrational energy to other modes ("intramolecular vibrational energy redistribution", IVR) takes place, which usually also prevents mode-selective photochemistry. Next to these processes, again IC processes can occur, which in the present case transfer the energy back into highly excited vibration states of the S_0 ground state.

It becomes obvious that many of the ultrafast processes have to do with the coupling of electronic and vibrational states. In order to study these dynamics vibration sensitive techniques have to be applied. An example is the transient infrared absorption. Another possibility is offered by the nonlinear Raman techniques discussed above.

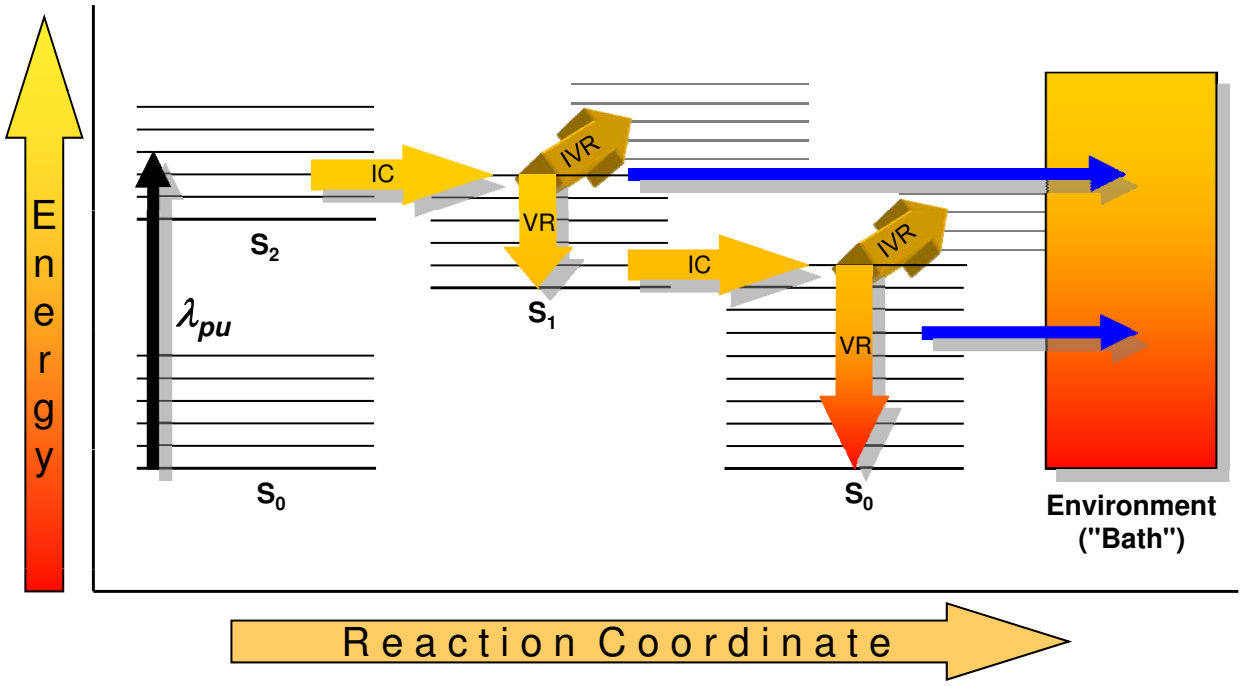

Figure 12: *Carotenoids are important parts of light harvesting complexes. Decisive for their contribution to the overall energy flow are their internal channels, which are indicated in this scheme. The photo excitation with* λ_{pu} *excites the molecules into their excited electronic* S_2 *state. An optical transition into the (dark)* S_1 *state is symmetry forbidden. Internal conversion (IC) nevertheless results in a population also of* S_1*. This non-Born Oppenheimer dynamics populates the* S_1 *state in hot vibrational states. Due to collisions with bath molecules a fast vibrational relaxation (VR) cools the molecule down along the ladder of vibration overtones. In addition to this, also intramolecular vibrational energy redistribution (IVR) between different modes takes place. Finally, the energy will be via IC transferred into hot vibrational states of the* S_0 *ground state where again VR and IVR result in energy dissipation and redistribution, respectively. If the molecule is coupled to e.g. a chlorophyll molecule, the intermolecular energy transfer between the different molecules will be strongly influenced by the internal dynamics.*

3.4.2 Pump-CARS experiment on β-carotene

In order to experimentally explore the role of different normal modes of a molecular system during a non-adiabatic process such as IC, a real-time, mode-selective monitor of the population flow must be employed. For this purpose, CARS can be used as a probe mechanism in a time-resolved pump-probe scheme [19] as shown in Fig. 13.

The mechanism, with which the CARS process can act as selective probe of the population within the vibrational states of a specific normal mode has its foundation in the strong enhancement of the CARS intensity in the case that the energy difference between the pump and Stokes lasers is resonant to a Raman transition. Furthermore, the energy level of the quantum state with $v = 0$ in the electronic ground state will not be uniform for different normal modes leading to an offset in the progression of energy levels ($v = 0, 1, 2, \ldots, n$) among the different normal modes. Therefore, a Raman resonance enhancement can only be fulfilled, if the CARS process takes place out of an initial vibrational state of the normal mode to which the energy difference is tuned to. The effect of an anharmonic potential on the energy gap between the vibrational states of a specific normal mode will be compensated by the broadband nature of the femtosecond laser pulses applied in the experiment. In summary, CARS as a probe mechanism is capable of acting as a filter for the interrogation of the progression of vibrational states ($v = 0$ to n) of a specific normal mode.

This selectivity is utilized for interrogating the population flow in normal modes of β-carotene subsequent to the S_1/S_0 IC using the experimental scheme shown in the left panel of Fig. 13. The relaxation dynamics from the S_2 into the S_1 state taking place after excitation with the initial pump laser (IP) into the S_2 state is very fast and can be studied *e.g.* by using a transient grating technique (see below). In order to resolve the dynamics of the subsequent population flow from the S_1 state into the different normal modes of the S_0 state, a variable delay time is introduced between the IP laser and the lasers of the CARS process. A typical transient is displayed on the top left of Fig. 13. The initial fast descent of the CARS intensity is due to the bleaching of the ground S_0 state by the IP at time zero. The recovery of the signal gives the desired information about the molecular dynamics.

By tuning the CARS process to different Raman modes of β-carotene in the electronic ground state and obtaining the respective transient, a superposition of the dynamics taking place in the vibrational states ($v = 0$ to n) of a specific normal mode can be observed. This population flow taking place as the result of the S_1/S_0 IC and subsequent IVR and VR can be characterized by a mono-exponential recovery time-constant. As result, recovery time constants can be assigned to the different normal modes. The results are summarized in the plot shown in the lower right panel of Fig. 13 as well as in the table given there. These data clearly show that the population flow from the S_1 state into the electronic ground state is not uniform for the normal modes that were interrogated. Here, the C=C stretch vibration is found to most efficiently couple the two electronic states S_1 and S_0. With this information, it is possible to gain direct insight into the exact mechanism of the IC with respect to the nuclear dynamics involved in this electronic transition.

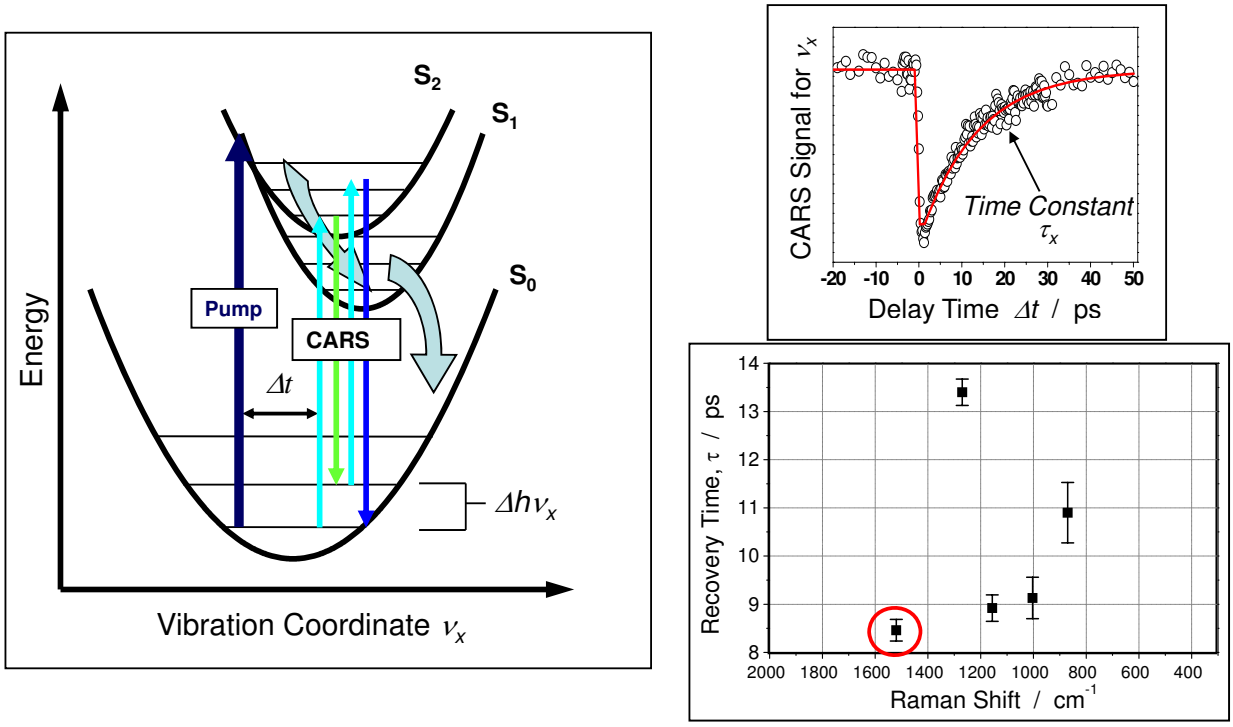

Raman Mode / cm^{-1}	Recovery Time τ / ps	Description
1524	8.46	C=C Symmetric Stretching
1269	13.40	C-H In Plane Bending with C-C Stretch
1157	8.92	C-C Symmetric Stretching
1006	9.13	Methyl to Chain Stretch
872	10.90	C=C-C Bending

Figure 13: *In order to follow the energy flow within the β-carotene molecule (compare Fig. 12) a combination of a single-pulse pump excitation and CARS probing can be used. Here, no change of the internal timing of the CARS laser pulses is applied. CARS merely serves as mode-selective probe. If the CARS lasers are chosen to be resonant with the* $S_2 \leftarrow S_0$ *absorption transition, selectively dynamics of vibrational states in the* S_0 *ground state can be observed. The participating optical transitions as well as the energy flow after pump excitation are indicated in the potential energy scheme of β-carotene on the left hand side. The right upper panel displays a typical transient observed as CARS signal as function of the delay time between pump laser pulse and CARS process. The fast descent of the signal at time zero is due to the depletion of the ground state population by the pump laser pulse. The signal recovery is caused by the different processes indicated in Fig. 12, which finally repopulate the* S_0 *ground state. The time constant* τ_x *of the recovery can be determined for every vibration mode* ν_x *in the ground state (right lower panel). From this, the most efficient coupling can be found for the C=C stretch vibration of the carotene chain (see table).*

3.4.3 Transient grating experiment on β-carotene

One degree of freedom for FWM spectroscopy mentioned in section 3.3 was beam geometry. We have seen that FWM can also be combined with an initial pump laser pulse to study the complex dynamics found in carotenoids. Now, we will use the same molecular system to demonstrate that using the laser pulses of the CARS process enables us also to perform a completely different experiment accessing these intra molecular processes.

In general, for the given combination of laser wavelengths different FWM processes are possible. With the same beam geometry used for the CARS experiment also a laser interaction is allowed, where pump and probe lasers perform a two photon absorption process into a high lying electronic state, from where the system is brought back into its initial state by the sequence of Stokes laser and anti-Stokes emission. Depending on resonance conditions and timing of the laser pulses, this process can give rise to an intense signal, which must not be neglected when discussing the experimental results. Just looking to the energy diagram, also a further FWM interaction can be given, which is called "transient grating" (TG) or "population grating" spectroscopy (a "virtual photon echo" technique). In Fig. 14, CARS and TG energy diagrams are compared to each other. In the TG process two photons (① and ②) couple the electronic ground and excited states. Due to the spatical overlap of the two coherent light fields, an interference pattern is written into the molecular ensemble modulating the spatial distribution of population in the respective states. The interaction with pulse ③, which in principle can have arbitrary wavelength, results in a scattering of this pulse following the Bragg conditions. Therefore, the signal is not frequency shifted relative to pulse ③ and can be found in well defined directions defined by the angle between the three laser pulses. Even when energetically possible, in a CARS experiment *e.g.* with a folded BoxCARS arrangement this process is not observed.

The reason for this is the geometric arrangement of the laser beams (phase matching), which is different for CARS and TG spectroscopy. Figure 15 shows on the left hand side the folded BoxCARS geometry of the CARS process together with a photo taken from lasers and anti-Stokes signal behind the sample. On the right hand side the arrangement of the lasers according to the requirements of the TG experiment is shown also assuming a folded BoxCARS geometry. The exchange of the positions of lasers ② and ③ (Stokes and probe) yields a signal, which now is not anti-Stokes shifted but rather has the frequency of the scattered laser ③.

For the femtosecond time-resolved experiments, in the TG scheme, the first two pump pulses (① and ②) interact simultaneously with the sample, preparing a transient grating of electronic ground and excited state molecules. The probe pulse (③) is delayed in time by Δt relative to the pump lasers, in order to interrogate the dynamics of the transient population. By choosing the color of the probe pulse to be in resonance with an electronic transition that can only be accessed by an excited state, it is possible to selectively observe the development in this exited state population while the dynamics of the electronic ground state do not contribute to the transient signal.

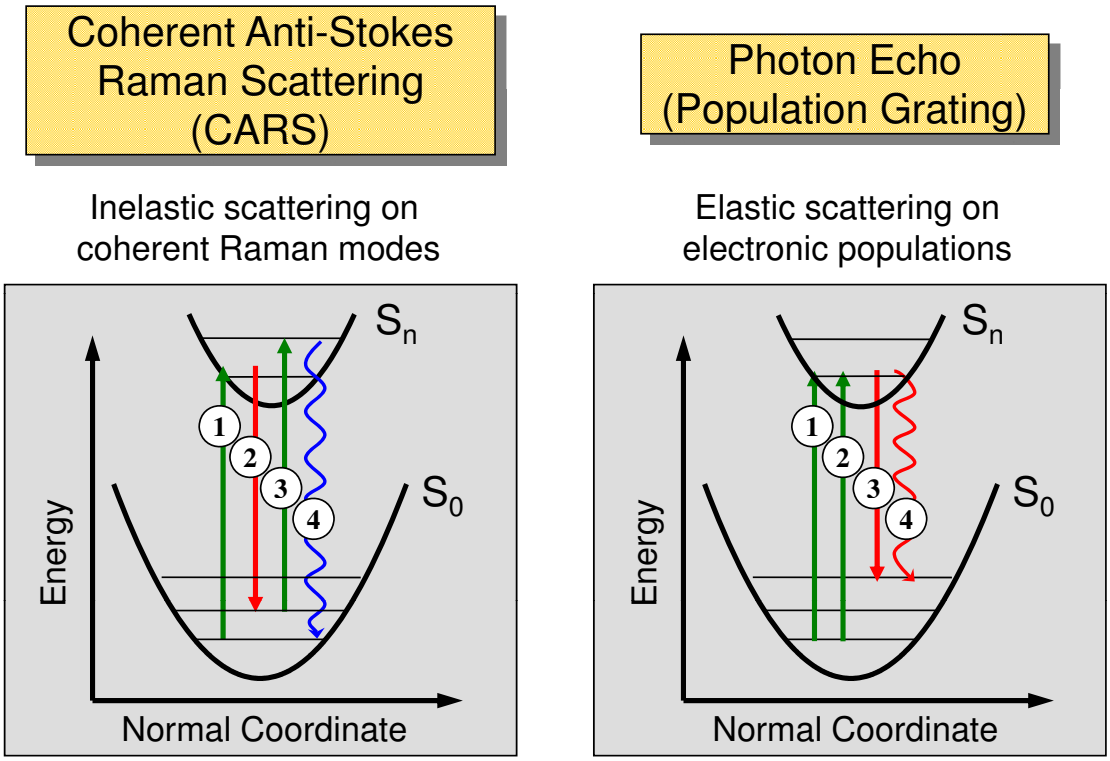

Figure 14: *The energy level diagrams compare two processes, which both can be induced by the interaction of the three lasers marked by ①, ②, and ③ in the scheme. On the left hand side, the CARS process is shown, where ① is the pump, ② the Stokes, and ③ the probe laser pulse. The signal ④ is anti-Stokes shifted relative to the probe laser wavelength. On the right hand side, a transient grating (TG) process is presented. Here, two lasers, ① and ②, of equal wavelengths write population gratings of electronic ground and excited states. The third pulse, ③, which acts as probe, is scattered from this grating according to the Bragg conditions giving rise to a signal ④ of equal wavelength.*

A theoretical description of the TG process will not be given here. Theory shows for the CARS process that the phase development described by T_2 determines the signal decay. In TG spectroscopy T_1 measuring the population life time is the only relevant time constant, since the two pump lasers prepare the same state:

$$I_{TG}(\Delta t) \propto e^{-2\Delta t/T_{1,e}} \,. \tag{15}$$

Depending on the chosen resonance conditions, $T_{1,e}$ refers to one or different electronic states (index e). The development leading to this equation can be described qualitatively in order to give a clearer picture of the TG scheme. The population prepared by the simultaneously acting pump pulses and scattering of the probe pulse can be seen as the scattering of a single laser pulse from a non-equilibrium population analog to a incoherent pump-probe scheme.

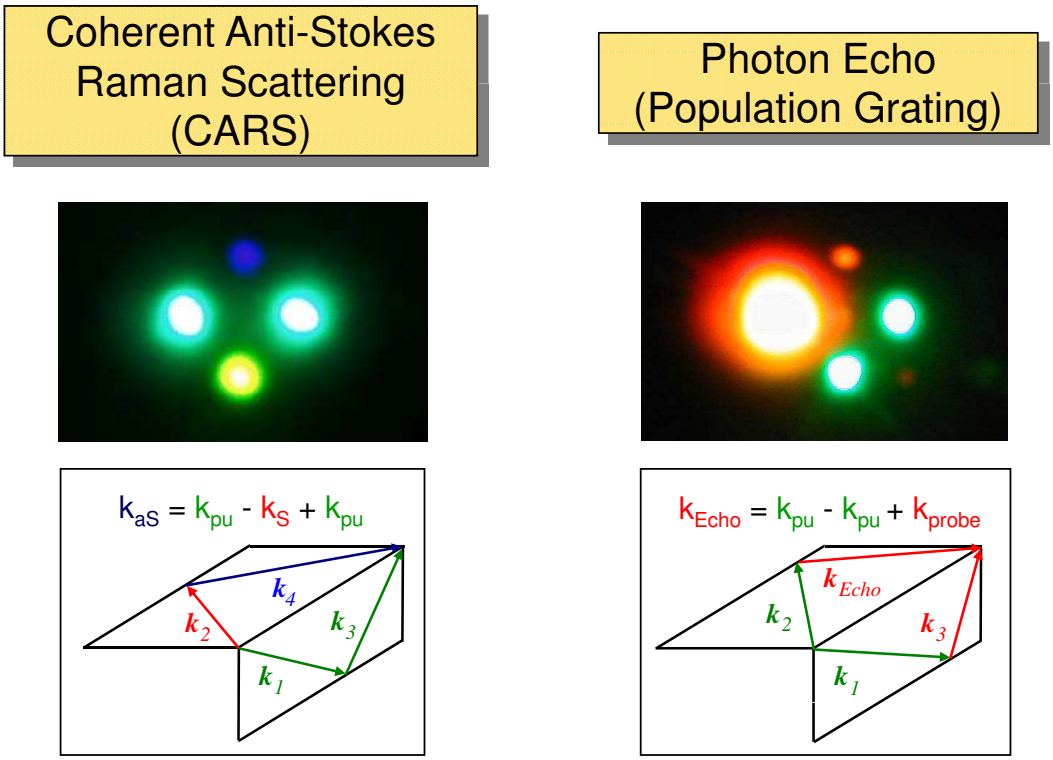

Figure 15: *The geometric arrangement of the laser beams decides on the resulting process. While the wave vector diagram on the left hand side produces the anti-Stokes signal of the CARS process, the exchange of lasers ② and ③ gives rise to transient grating scattering (right hand side). The photos show lasers and signals for both schemes. For the TG experiment the probe laser ③ was slightly red-shifted compared to the Stokes laser of the corresponding CARS process in order to better fulfill resonance conditions.*

Here, the only fundamental difference to the classical pump-probe scheme is rooted in the preparation of an excited population grating by the two pump lasers rather than the simple population, exited by the single pump laser in a pump-probe scheme. This allows for an elastic Bragg scattering of the probe pulse off the excited state population grating with the detection of an optically coherent signal (where the homodyne detection of a quadrature detector leads to a quadratic proportionality of the population to the signal intensity) rather than the incoherent signal of a pump-probe scheme (where the signal is linearly proportional to the population) [20, 21].

As example, an experiment is introduced in the following, where femtosecond time-resolved TG is used to study the dynamics in the excited S_1 state of β-carotene [22]. Figure 16 shows a schematic potential energy diagram of β-carotene with the optical transitions involved in the TG process.

The TG experiment yields a characterization of the dynamics of the IC that couples the S_1

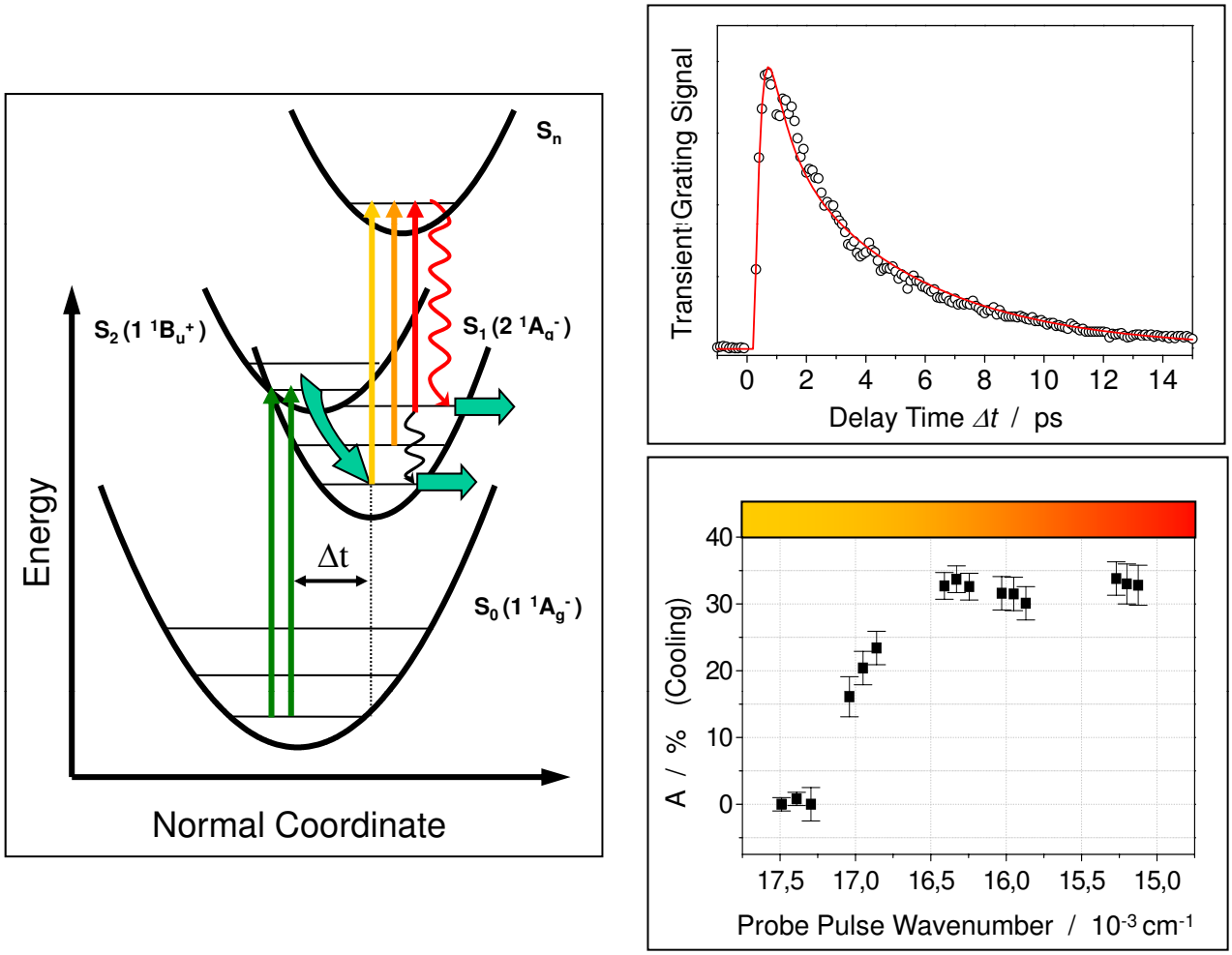

Figure 16: *The energy flow within the β-carotene molecule (compare Fig. 12) can be also followed by directly accessing the dark state S_1. For this the two pump lasers first write a transient population grating for molecules excited into their S_2 state. In order to selectively investigate the transfer of this grating into the S_1 state due to IC, the probe laser is made resonant with the $S_n \leftarrow S_1$ transition. To access ground and hot vibration states, the probe wavelength is varied at the red edge of this transient absorption. The energy level diagram on the left indicates the different laser interactions as well as the dynamics observed by the TG technique. On the right hand side a typical transient is shown, which was fitted (red curve) using Equ. 16 yielding the contribution of vibrational cooling to the decay of the TG signal, A. The experiment is repeated for different probe photon energies. As a result, A is plotted as a function of the probe wavenumber. From this, a faster rate for the S_1/S_0 IC for vibrationally excited states could be determined.*

and electronic ground state S_0 of β-carotene. At time zero gratings of the S_2 state population are induced in the sample space by focusing two non-collinear pump lasers pulses (λ_{pu} = 510 nm) into the sample in resonance with the $S_2 \leftarrow S_0$ optical transition in β-carotene. The subsequent S_2/S_1 internal conversion allows for population flow into the S_1 state, generating a grating of S_1 state molecules. While the two pump pulses interact simultaneously with the sample, a third probe pulse (λ_{probe} = 570 to 635 nm) resolves the dynamics of the S_1 state with the help of a variable time delay, Δt between the grating formation by the two pump pulses and the interrogation with the probe pulse. The probing of the S_1 state is accomplished by elastically scattering the probe pulse under Bragg conditions off the grating in resonance to the $S_n \leftarrow S_1$ optical transition in β-carotene where S_n is a higher lying singlet state. The transient grating signal is directed into a monochromator and the spectral components of the signal are detected with a multichannel CCD detector. The intensity of the different spectral channels in the signal is recorded as a function of the delay time, Δt. This allows for the population flow from the originally prepared S_2 state into the S_1 state through the S_2/S_1 IC, and the subsequent depopulation of the S_1 state by means of the S_1/S_0 IC to be observed. Since the S_2 state lies approximately 6000 cm^{-1} above the S_1 state, the S_2/S_1 IC prepares vibrationally hot modes in the S_1 state. In order to monitor the population flow in different regions of the S_1 potential, the central wavelength of the probe pulse is varied from 570 to 635 nm to include spectral positions that lie red-shifted to the $S_n \leftarrow S_1$ transition. This allows for vibrational ground state modes to be monitored when the probe laser is in resonance with the S_1 absorption while red-shifting out of the absorption profile brings the probe laser pulse in resonance with vibrationally hot states of the S_1 potential.

A typical transient is displayed on the left hand side of Fig. 16. In order to evaluate the resonant transient data, a model can be formulated that includes the possible population and depopulation channels for the region of the S_1 potential that is monitored by the probe pulse. For this, the S_2/S_1 IC is assumed to be the only mechanism by which the S_1 state is populated. This process is characterized by a time constant, τ_{S_2/S_1}. For molecules in the vibrational ground state of the S_1 potential, the S_1/S_0 internal conversion is assumed to be the only channel of depopulation and this process is characterized by the time constant, τ_{S_1/S_0}. Fluorescence as a decay channel for S_1 state molecules can be neglected since, as mentioned above, the $S_1 \leftarrow S_0$ optical transition is symmetry forbidden. For wavelengths of the probe laser that are red-shifted to the S_1 state absorption, vibrationally hot states are also interrogated by the probe laser pulse. In this case, two possible decay channels can be assumed that allow molecules to leave the region of the S_1 potential that is accessed by the probe laser. The first channel is the S_1/S_0 IC taking place out of vibrationally hot states. The second channel is given by vibrational cooling (VR) due to system-bath coupling, resulting in energy transfer to solvent molecules. The cooling processes are described with a global time constant for all modes, τ_{cool}. These assumptions for the S_1 state dynamics in combination with the time dependency of a transient grating signal result in the following model for the resonant transient data:

$$I_{TG}(\Delta t) = \left|(1 - e^{-\Delta t/\tau_{S_2/S_1}}) \cdot \left[A e^{-\Delta t/\tau_{cool}} + (1 - A) e^{-\Delta t/\tau_{S_1/S_0}}\right]\right|^2 \qquad (16)$$

Using Equ. 16 to fit the TG transient curves for different probe photon energies yields a plot of A versus probe wavenumber (see lower right panel of Fig. 16). The fit parameter A describes the distribution between cooling and the S_1/S_0 IC as a decay channel out of the probe window. From this a faster rate for the S_1/S_0 IC for vibrationally excited states could be determined.

4 Conclusion

This short lecture only gives a small insight into the huge number of different techniques, which where developed to study even complex molecular dynamics. Instead of presenting a long list of methods with a short description for each of them, I have decided to demonstrate the basic ideas selecting some linear and nonlinear spectroscopy approaches and discussing real applications. Special emphasis was put on nonlinear four-wave mixing techniques, which are powerful tools due to their many degrees of freedom. Only some of the possible variations have been discussed here. It is in many cases also up to the invention of the experimenter to develop new variations best adapted to a specific problem. Even having many methods at hand, still much effort has to be put into research. Future might bring even more advanced techniques for the study of *e.g.* biologically or medically relevant systems.

References

[1] H. Eyring, M. Polanyi, Z. Phys. Chem. B 12 (1931) 279.

[2] H. Eyring, J. Chem. Phys. 3 (1935) 107.

[3] M. G. Evans, M. Polanyi, Trans. Faraday Soc. 31 (1935) 875.

[4] R. G. W. Norrish, G. Porter, Nature 164 (1949) 658.

[5] C. V. Shank, E. P. Ippen, Appl. Phys. Lett. 24 (1974) 373.

[6] M. J. Rosker, M. Dantus, A. H. Zewail, Science 241 (1988) 1200.

[7] P. Anfinrud, F. Schotte, Science 309 (2005) 1192.

[8] C.-Y. Ruan, V. A. Lobastov, F. Vigliotti, S. Y. Chen, A. H. Zewail, Science 304 (2004) 80.

[9] T. S. Rose, M. J. Rosker, A. H. Zewail, J. Chem. Phys. 88 (1988) 6672.

[10] T. S. Rose, M. J. Rosker, A. H. Zewail, J. Chem. Phys. 91 (1989) 7415.

[11] A. Materny, T. Chen, A. Vierheilig, W. Kiefer, J. Raman Spectrosc. 32 (2001) 425.

[12] W. Kiefer, H. J. Bernstein, H. Wieser, M. Danyluk, J. Molec. Spectrosc. 43 (1972) 393.

[13] D. Lee, A. C. Albrecht, in: R. J. H. Clark, R. E. Hester (Eds.), Advances in Infrared and Raman Spectroscopy, Vol. 12, J. Wiley & Sons, Chichester, 1985, p. 179.

[14] D. Lee, A. C. Albrecht, in: I. Prigogine, S. A. Rice (Eds.), Adv. Chem. Phys., Vol. 83, J. Wiley & Sons, Chichester, 1993, p. 43.

[15] S. Meyer, M. Schmitt, A. Materny, W. Kiefer, V. Engel, Chem. Phys. Lett. 281 (1997) 332.

[16] S. Meyer, V. Engel, J. Phys. Chem. A 101 (1997) 7749.

[17] E. T. J. Nibbering, H. Fidder, E. Pines, Annu. Rev. Phys. Chem. 56 (2005) 337.

[18] V. Sundström, T. Pullerits, R. van Grondelle, J. Phys. Chem. B 103 (1999) 2327.

[19] T. Siebert, M. Schmitt, V. Engel, A. Materny, W. Kiefer, J. Am. Chem. Soc. 124 (2002) 6242.

[20] H. J. Eichler, P. Gunter, D. W. Pohl, Laser Induced Dynamics Gratings, Springer, Berlin, 1986.

[21] T. Siebert, Ph.D. thesis, University of Würzburg (2002).

[22] T. Siebert, V. Engel, A. Materny, W. Kiefer, M. Schmitt, J. Phys. Chem. A 107 (2003) 8355.